AD-A158 318 DROPLET SIZING RESEARCH(U) SPECTRON DEVELOPMENT LABS INC COSTA MESA CA C F HESS 15 APR 85 SDL-85-2286-12 AFOSR-TR-85-0562 F49620-83-C-0060 1/1

UNCLASSIFIED F/G 14/2 NL

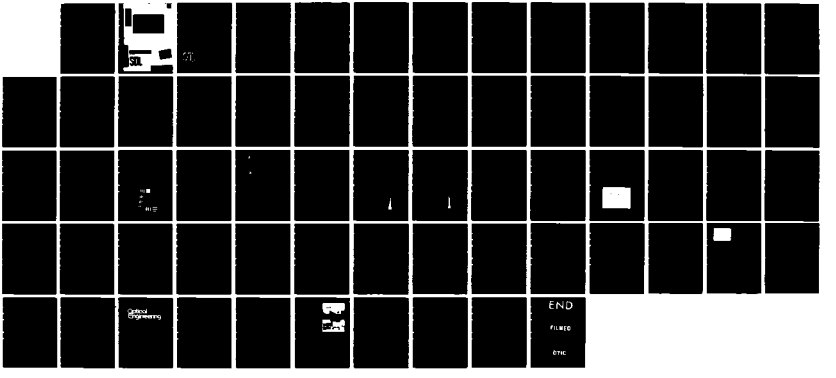

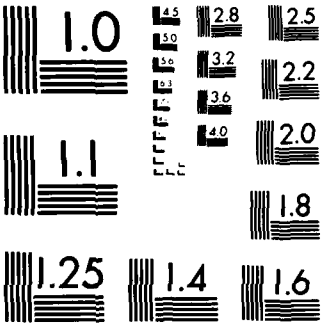

MICROCOPY RESOLUTION TEST CHART

DROPLET SIZING RESEARCH

ANNUAL REPORT

SDL No. 85-2286-12

15 April 1985

AFOSR-TR- 85-0562

DROPLET SIZING RESEARCH

ANNUAL REPORT

SDL No. 85-2286-12

15 April 1985

Approved for public release;
distribution unlimited.

Prepared For:

Air Force Office of Scientific Research
Dr. Leonard Caveny
AFOSR/NA
Directorate of Aerospace Sciences
Building 410
Bolling AFB, DC 20332

Under Contract No.

F49620-83-C-0060

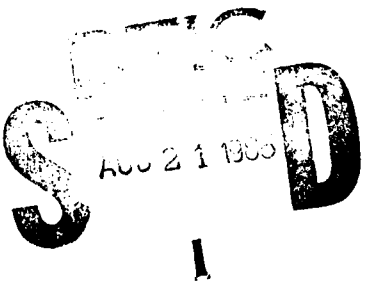

SDL
SPECTRON DEVELOPMENT LABORATORIES, INC.
3303 HARBOR BLVD., SUITE G-3, COSTA MESA, CA 92626 • (714) 549-8477

Approved for public release;
distribution unlimited.

UNCLASSIFIED
SECURITY CLASSIFICATION OF THIS PAGE

AD-A158318

REPORT DOCUMENTATION PAGE

1a. REPORT SECURITY CLASSIFICATION UNCLASSIFIED	1b. RESTRICTIVE MARKINGS
2a. SECURITY CLASSIFICATION AUTHORITY	3. DISTRIBUTION/AVAILABILITY OF REPORT Approved for Public Release; Distribution is Unlimited.
2b. DECLASSIFICATION/DOWNGRADING SCHEDULE	
4. PERFORMING ORGANIZATION REPORT NUMBER(S) 85-2286-12	5. MONITORING ORGANIZATION REPORT NUMBER(S) AFOSR-TR- 85-0562
6a. NAME OF PERFORMING ORGANIZATION Spectron Development Labs. / 6b. OFFICE SYMBOL (If applicable)	7a. NAME OF MONITORING ORGANIZATION AIR FORCE OFFICE OF SCIENTIFIC RESEARCH
6c. ADDRESS (City, State and ZIP Code) 3303 Harbor Blvd., Ste. G-3 Costa Mesa, CA 92626	7b. ADDRESS (City, State and ZIP Code) BOLLING AFB DC 20332-6448
8a. NAME OF FUNDING/SPONSORING ORGANIZATION Air Force Office of Scientific Research / 8b. OFFICE SYMBOL (If applicable) NA	9. PROCUREMENT INSTRUMENT IDENTIFICATION NUMBER F49620-83-C-0060
8c. ADDRESS (City, State and ZIP Code) Bolling Air Force, DC 20332-6448	10. SOURCE OF FUNDING NOS.

PROGRAM ELEMENT NO.	PROJECT NO.	TASK NO.	WORK UNIT NO.
61102F	2308	A3	

11. TITLE (Include Security Classification)
Droplet Sizing Research

12. PERSONAL AUTHOR(S)
Hess, Cecil F.

13a. TYPE OF REPORT	13b. TIME COVERED	14. DATE OF REPORT (Yr., Mo., Day)	15. PAGE COUNT
Annual	FROM 1-15-84 TO 1-15-85	1985, 4, 15	44

16. SUPPLEMENTARY NOTATION

17. COSATI CODES			18. SUBJECT TERMS (Continue on reverse if necessary and identify by block number)
FIELD	GROUP	SUB. GR.	droplet sizing, particle velocity, mass flux, nonintrusive, advanced laser diagnostics.

19. ABSTRACT (Continue on reverse if necessary and identify by block number)

A method to measure the size and velocity of individual particles in a flow is discussed. Results are presented for controlled monodisperse sprays and compared to flash photographs. Typical errors between predicted and measured sizes are less than 5%. Experimental results of the probe volume size are satisfactorily compared to a theoretical algorithm. A very simple optical apparatus is described and used to characterize a spray produced by a simplex nozzle. The size distribution and the Sauter mean diameter of this spray are presented as a function of position and pressure.

20. DISTRIBUTION/AVAILABILITY OF ABSTRACT	21. ABSTRACT SECURITY CLASSIFICATION
UNCLASSIFIED/UNLIMITED ☒ SAME AS RPT. ☐ DTIC USERS ☐	Unclassified

22a. NAME OF RESPONSIBLE INDIVIDUAL	22b. TELEPHONE NUMBER (Include Area Code)	22c. OFFICE SYMBOL
LEONARD H CAVENY	(202) 767-4937	AFOSR/NA

DD FORM 1473, 83 APR EDITION OF 1 JAN 73 IS OBSOLETE.

UNCLASSIFIED
SECURITY CLASSIFICATION OF THIS PAGE

TABLE OF CONTENTS

NO.		PAGE
1.0	INTRODUCTION.....	1
2.0	STATEMENT OF WORK.....	2
2.1	Year 1 - Droplet Measurement Research	2
2.2	Year 2 - Droplet Measurement Research	3
2.3	Year 3 - Droplet Measurement Research	3
3.0	DESCRIPTION OF OPTICAL TECHNIQUE.....	5
3.1	Apparatus and Experimental Facility.....	9
3.2	Experimental Determination of the PIMAX Probe Volume.....	14
3.3	Polarization Crosstalk.....	17
4.0	EXPERIMENTAL RESULTS.....	21
4.1	Pre-Calibration Procedure.....	21
4.2	Dynamic Size Range.....	29
4.3	Spray Measurements Procedure.....	29
4.4	Spray Results.....	32
5.0	PUBLICATIONS.....	39
6.0	PROFESSIONAL PERSONNEL.....	40
APPENDIX A	"Nonintrusive Optical Single-Particle Counter Measuring the Size and Velocity of Droplets in a Spray," C. F. Hess, Applied Optics, 1984.	41
APPENDIX B	"Spray Characterization with a Nonintrusive Technique using Absolute Scattered Light," C. F. Hess and V. E. Espinosa, Optical Engineering, 1984.	50

LIST OF FIGURES

NO.		PAGE
1.	Schematic of the PIMAX breadboard	6
2.	Schematic of PIMAX system with compact transmitter	13
3.	Comparison between experimental and theoretical probe volume characteristic dimension	16
4.	Schematic of Photographic System	23
5.	Photograph of resolution chart	23
6a.	Photograph of 80μm droplet string	25
6b.	Photograph of 52μm droplet string	25
6c.	Photograph of 52μm droplet spray	25
7a.	Size and Velocity of a monodisperse string of droplets measured with PIMAX	27
7b.	Size and velocity histograms of a monodisperse spray (with some doublets) measured with PIMAX	27
8	Size and velocity histograms of a monodisperse spray of 58μm droplets	28
9	Oscilloscope trace of signals produced by a monodisperse string of droplets	31
10a.	PIMAX measurements of a spray at a radial position of 0mm and axial position of 50mm: uncorrected	34
10b.	PIMAX measurements of a spray at a radial position of 0mm and axial position of 50mm: probe volume corrected	34
11a.	PIMAX measurements of a spray at a radial position of 10mm and axial position of 50mm: uncorrected	36
11b.	PIMAX measurements of a spray at a radial position of 10mm and axial position of 50mm: probe volume corrected	36
12a.	Variation of characteristic diameter of spray with radial position and pressure: peak diameter	37
12b.	Variation of characteristic diameter of spray with radial position and pressure: Sauter mean diameter	37

ABSTRACT

A method to measure the size and velocity of individual particles in a flow is discussed. Results are presented for controlled monodisperse sprays and compared to flash photographs. Typical errors between predicted and measured sizes are less than 5%. Experimental results of the probe volume size are satisfactorily compared to a theoretical algorithm. A very simple optical apparatus is described and used to characterize a spray produced by a simplex nozzle. The size distribution and the Sauter mean diameter of this spray are presented as a function of position and pressure.

1.0 INTRODUCTION

This second annual report describes the work conducted under Contract No. F49620-83-C-0060 during the period 15 January 1984 to 15 January 1985.

During this second year of the contract all the work has been conducted with the "maximum intensity technique", since it was concluded that this technique was far superior to the visibility/intensity for spray measurements. A modified version using beams with normal polarizations was introduced and tested with several types of sprays. The probe volume algorithm developed last year was verified experimentally, and is shown to be an important aspect of the measurements.

The experimental evidence substantiates that the "maximum intensity technique" is a powerful technique for measuring the size and velocity of droplets.

Included as an appendix are two papers which resulted from this work. These papers have sections of references to relevant works.

2.0 STATEMENT OF WORK

The statement of work as shown in the original proposal and contract is included here for the three years of the contract. Next to each task there is an asterisk (*) or a triangle (Δ), the asterisk indicating completion of the task and the triangle indicating that some work was done during this year.

2.1 Year 1 - Droplet Measurement Research

*Task 1.0 - Evaluation and assessment of previous results to provide a basis of departure for the present research.

*Task 2.0 - Plan the research to study two advanced droplet sizing concepts (V/I and IMAX) both analytically and experimentally.

*Task 3.0 - Theoretical definition of the two concepts based on fundamental scattering theories.

*Task 4.0 - Breadboard experimental setups to test and study both techniques.

*Task 5.0 - Experimentally determine the intensity of the light scattered by droplets immersed in a Gaussian beam. Compare these results with present scattering theories and correlations.

*Task 6.0 - Explore signal characteristics of the two techniques under ideal conditions, and establish optimum regions of validity.

*Task 7.0 - Analyze above data and compare to the theoretical description obtained in Task 3.0, to determine optimum selection of parameters.

*Task 8.0 - Report the results of each of the program tasks and develop a publication for submittal to a referee journal.

2.2 Year 2 - Droplet Measurement Research

*Task 1.0 - Evaluate and assess previous year's results and recent relevant developments and re-establish the direction of the proposed investigation.

*Task 2.0 - Plan the research for the second year based on information obtained to this point.

*Task 3.0 - Formulate an analytical model to compute the optical probe volume and check experimentally verify the result.

*Task 4.0 - Explore the signal characteristics of a monodispersed spray when laser beams are interfered by a real spray.

*Task 5.0 - Evaluate how regions of established validity under ideal conditions are affected by beam blockage.

Task 6.0 - Formulate statistical analysis to predict the effect of spray blockage on signal characteristics.

*Task 7.0 - Define and establish a processing method for the concepts studied. Perform preliminary spray measurements.

Task 8.0 - Analyze above data and compare to the statistical model obtained in Task 6.0 to reassess the validity of the optimum parameters obtained under ideal conditions.

*Task 9.0 - Report the results of each of the program tasks and develop a publication for submittal to a referee journal.

2.3 Year 3 - Droplet Measurement Research

*Task 1.0 - Ev 'uate and assess developments and the results of the first two years and redefine the critical aspects of the research.

ΔTask 2.0 - Plan the research for the third year based on available information. Consider alternative methods or new concepts.

*Task 3.0 - Perform measurements in real sprays and explore the signal characteristics and establish the limitations of the techniques.

ΔTask 4.0 - Test processing methods chosen during second year, in the presence of real sprays, and develop corrections if necessary.

ΔTask 5.0 - Compare the results obtained with the various methods for the same spray under various spray conditions.

Task 6.0 - Analyze above data in conjunction with statistical models to establish the limitations of the techniques.

ΔTask 7.0 - Report the results of the entire program and develop a publication for submittal to a referee journal.

3.0 DESCRIPTION OF OPTICAL TECHNIQUE

The method discussed here bases the size measurement on the absolute intensity scattered by the particle crossing the probe volume, and the velocity measurement on the classical Doppler signal. In situ single particle counters are limited because of the nonuniform profile (typically Gaussian) of laser beams. Under this condition a particle crossing the middle of the beam will scatter more light than a similar particle crossing through the edge. Therefore, the relationship between size and scattered light is not unique.

To circumvent this problem, two small beams of a given wavelength or polarization are crossed in the middle of a larger beam of different wavelength or polarization identifying a region of almost uniform intensity and, therefore, removing the Gaussian ambiguity. The crossing beams will interfere and a fringe pattern will be formed in the middle of the large beam (Figure 1). Signals exhibiting an ac modulation correspond to particles that cross the fringe pattern and therefore, the middle of the large beam. Both size and velocity of individual particles can be extracted from this signal. This method was presented in great detail in the 1984 annual report for a two-color laser system (the IMAX technique). It is shown here that the technique can be implemented with a single-color laser by dividing its polarization into two normal components. For simplicity and as an extension to the IMAX it is referred to as PIMAX.

If we refer to the small beam as 1 and the large beam as 2, the intensity profiles in the probe volume can be separated by their polarization and given by:

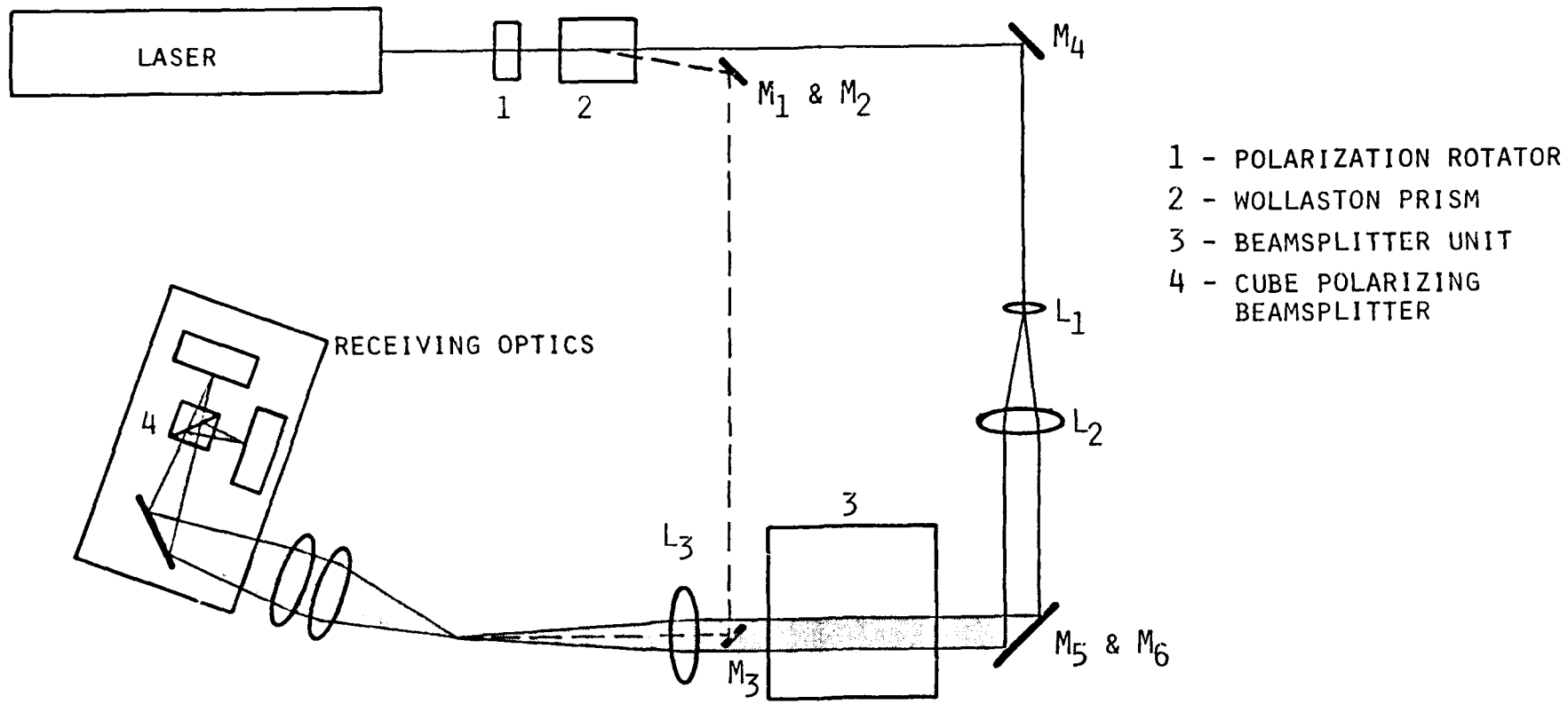

Figure 1. Schematic of the PIMAX breadboard: (1) polarization rotator; (2) Wollaston prism; (3) beam splitter unit; (4) cube polarizing beam splitter.

Typically R_1 is .04 to .08 for I_{SL}= 3 to 6. This will result in a size error of 2 to 4%. Obviously this error can be reduced by reducing I_{SL}, this, however, will impact the signal to noise ratio of the SPMT which establishes the detectability of the signal. R_2 was negligible in all the experiments yet one must be aware that it would increase by reducing I_{SL}. Finally, it should be noticed that the cube polarizer (CP) of the receiver will influence the above results. It is 98% efficient for linearly polarized light, and 50% for unpolarized light. Thus, any unpolarized scattered light will be split into S and P components and be measured by both PMTs. If a beam splitter was used, the unpolarized scattered light would be unpolarized after the beamsplitter and most of it would be rejected by the polarization filter in front of the PMTs. The tradeoff is that each PMT would collect only 50% of the polarized light (compared to 98% with a CP).

In summary unlike the IMAX technique, the PIMAX is subject to crosstalk which need to be considered in the optical design. In our configurations this crosstalk was about 4 to 8% resulting in a 2 to 4% error in the size. This error could be virtually eliminated by placing the receiver on the plane of the laser beams thus reducing the ellipticity of the polarization.

the axis of the receiver. This direction was about 2° off the horizontal which is roughly half the crossover angle. Similar measurements of the light scattered from the large beam indicated that the principal direction of polarization was still vertical.

Notice that the change in the polarization described above can be virtually eliminated by placing the receiving optics on the plane of the laser beams. That is, elevated an angle θ from the optical table.

The next set of measurements consisted in analyzing the scattered light with the receiver. The PIMAX method presumes that the light scattered from a beam with S polarization can be separated from the light scattered from another beam with P polarization, and both can be separated and measured in separate photomultipliers. In our configuration (Figure 2) the photomultiplier referred to as BPMT is intended to measure only S polarized light, while SPMT only P polarized light. Referring to Figure 2, the light scattered by the particles crossing the probe volume is collected and focused by lenses L_6 and L_7 and separated into its two polarization components by CP. To test the crosstalk between the two polarizations a string of monodisperse droplets flowing through the probe volume was measured. The large and small beams were alternatively blocked and the signal was measured in both PMTs. Thus, we established how much of the light scattered from the small beams is measured on the BPMT and vice versa. The parameters of interest are the ratio for the pedestal of the small beam to the pedestal of the large beam as measured on BPMT (R_1) and the inverse ratio measured on SPMT (R_2). Notice that these ratios will be directly proportional to the relative peak intensities of the small to large beams in the probe volume (I_{SL}).

values were 180 for the small beams and 8000 for the large beams. Values in excess of 100:1 are adequate. To study the effect of particle interference a spray was used to block the laser beams. The attenuation of the beam was up to 30%. The polarization ratio of the small and large transmitting beams going through the spray was measured again. These values were typically 180 for the small beams and 4000 for the large one. These results indicate that there is no measurable unpolarization of the beams transmitted through a droplet field. This is not surprising since the light scattered along the transmitted beams will have the same polarization as the incident radiation. The second reason and their causes of depolarization were difficult to separate and were combined in the measurements.

In our present configuration the large and small beams form a plane perpendicular to the optical table. The receiving optics are on the optical table such that the scattering plane, defined by the large beam and the optical axis of the receiving optics, is parallel to the optical table. Since the small beams cross at the angle (γ) the scattering plane of these beams is at an angle with the optical table. The polarization of the large beam is perpendicular to the optical table, and the polarization of the small beams is parallel. This configuration will result in some ellipticity in the polarization of the light scattered from the small beams. The light scattered from the large beam will be linearly polarized along the diameter of the receiving lens parallel to the optical table. It will be slightly elliptical anywhere else. The principal direction of the polarization of the light scattered from the small beams was measured with a polarization filter along

Figure 3 are the average of y_{small} and y_{large}, and the theoretically predicted value. It can be deducted from this figure that there is a good agreement between the theoretical and the average experimental values.

3.3 Polarization Crosstalk

The accuracy of the PIMAX technique can be reduced if the scattered light is elliptically polarized and the polarization separators are not efficient. In a two-color system the separation of the colors is trivial and the problem of crosstalk need not be considered. In the two-polarization system care must be exercised to minimize this crosstalk. There are three reasons that can unpolarize the signal, therefore, reducing the separation. They are: 1) particles disturbing the laser beam; 2) scattering plane can be at an angle other than 0° or 90° with the incident polarization; 3) polarization separators are inefficient. This crosstalk was shown to be very small in the PIMAX system accounting for about 3% error in the particle size and have no measurable effect in the velocity.

Several tests were conducted to establish the reasons and level of the crosstalk. First the PIMAX transmitter was carefully aligned and the optical elements were free of stress which could introduce birefringence. The polarization rotator (PR of Figure 2) was carefully aligned by observing the interference between the large beam and any of the small beams. In the absence of fringes the polarizations of the large and small beams were normal to each other. The polarization ratio of the small beams and the large beam were then measured. Typically these

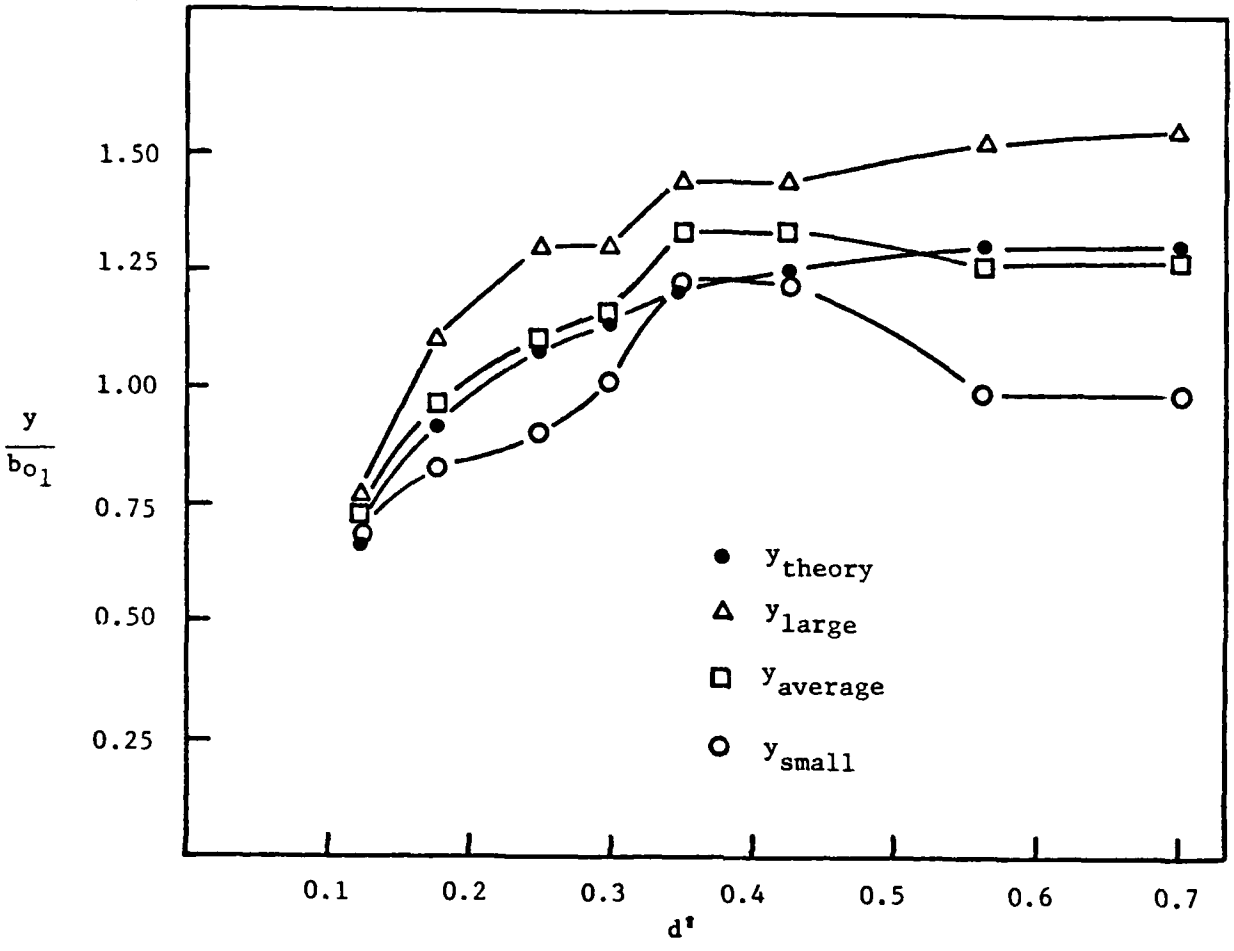

Figure 3. Comparison between experimental and theoretical probe volume characteristic dimension.

A very difficult part of this experiment was determining the edge of the probe volume for any particular size droplet. Theoretically, the edge of the probe volume is calculated by the expression given for y. Experimentally, there is a region near the edge of the PV where the rate of acquistion drops off. That is some of the signals (droplets) are processed by the electronics and some are not. The electronics impose an upper limit on the data rate of about 6 KHz, while the drops can be generated at a frequency of up to 60 KHz.

In defining the edge of the probe volume the data rate of signal acceptance was observed. One criterion corresponded to the location where the data rate dropped to about 90% of the maximum rate. Another criterion corresponded to a data rate very close to zero. Notice that in principle all the measured droplets are identical and traveling exactly through the same trajectory. Therefore, the data rate should be either zero or have a fixed constant value. In actuality the droplet trajectory can change by a few microns, therefore, causing some droplets to cross inside the probe volume while others cross outside. In addition, the droplets could vary in size, although we have no evidence of this.

The droplet generator was traversed from the position of peak intensity to the position of 90% data rate, and then zero data rate. The respective relative movements were recorded in each case. The 90% data rate corresponds to a conservatively small probe volume referred to in Figure 3 as y_{small}, while the zero data rate corresponds to a conservatively large probe volume and is indicated as y_{large}. Also shown on

The outputs of the photomultipliers are input to an electronic breadboard which measures the Doppler period and the peak intensity of each scattering center. A descripton of the electronics was given in the 1984 annual report.

3.2 Experimental Determination of the PIMAX Probe Volume

In optical probe volumes with nonuniform intensity distribution droplets that scatter light with large modulation are detectable over a larger region than those that scatter light with little modulation. As a result, the probe volume or region of detectablity is a function of droplet size. The derivation of the equation that relates the size dimension y of the probe volume to the droplet diameter d was given in last year's annual report on the IMAX system. This equation restated here, is now experimentally verified. It is given by:

$$y < \sqrt{\frac{-b_{0_1}^2}{2} \ln\left[\frac{I_{min}}{2I_{max}} \left(\frac{d_o}{d}\right)^2 \left(\frac{1+V_o}{v}\right)\right] - b_{0_1}^2}$$

To experimentally measure the y dimension of the probe volume in the scattering plane and perpendicular the transmitted laser beams, the Berglund-Liu droplet generator was used. This produced a steady and stable string of monodispersed water droplets as was also previously discussed in last year's report. The droplet generator was mounted on a precision x-y micrometric traverse so that the droplets could be positioned anywhere in the probe volume. The orifice of the B-L generator was placed as close to the probe volume as possible to minimize errors due to wander of the string of droplets; data was also repeated several times to reduce errors even further.

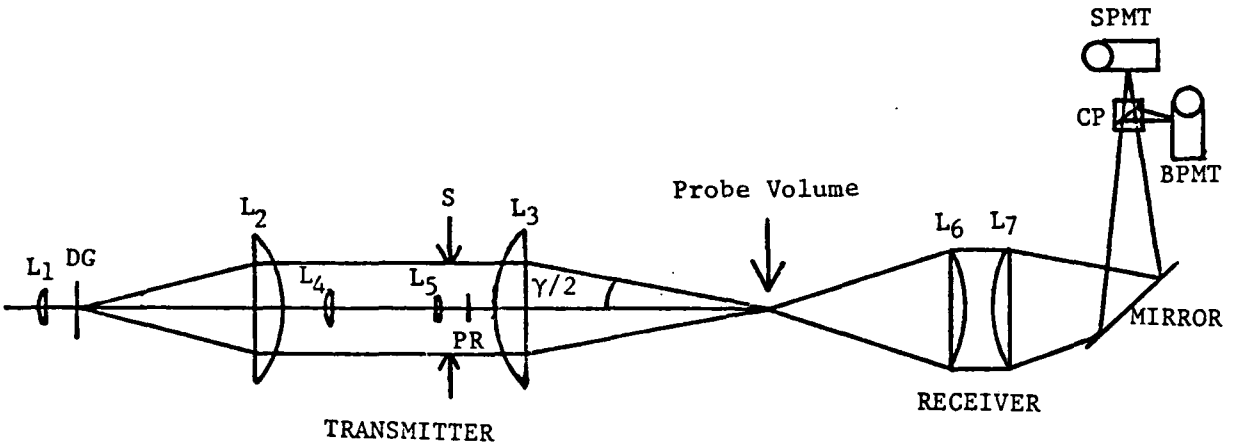

Achromatic Lens	Focal Length (mm)
L_1	35
L_2	220
L_3	500
L_4	112
L_5	16
L_6	300
L_7	500

CP: Cube Polarizer

DG: Diffraction Grating
100 lines/mm

PR: Polarization Rotator

Figure 2. Schematic of PIMAX system with compact transmitter.

parameter m. This expanded beam is then split into two beams with a compensated beam splitter. The transmitting lens L_3 focuses and crosses these two beams (which will be referred to as small beams because of their size at the probe volume relative to the third beam), thus forming an interference pattern of fringes in the middle of the big beam.

The scattered light collected by the receiver is separated into the P and S components by a cube polarizing beam splitter and is focused on pinholes in front of two identical PMTs. Interference filters are used to eliminate background light from other sources. To simplify the alignment a second, more compact breadboard was also built.

Figure 2 shows a schematic of this optical system, which consists of a transmitter and a receiver positioned 5° off axis. The transmitter uses a 5 mw He-Ne laser which is focused on a diffraction grating (DG) by lens L_1, and the three major orders are collimated by lens L_2. The zero order beam goes through a beam compressor formed by L_4 and L_5 and its polarization is rotated by PR. Lens L_3 focuses and crosses all three beams to form the probe volume. The light scattered by particles crossing the probe volume is collected by the same receiving optics as shown on Figure 1. The scattered light is collected by L_6 and focused onto the photomultipliers by L_7. A cube polarizer (CP) divides efficiently the scattered light into its two polarization components. In addition, a polarization filter was placed in front of the PMT which looks at the big beam (BPMT) to reduce the cross talk between the two polarizations.

TABLE 1. INTENSITY VERSUS SIZE (Continued)

BIN NO.	d'_{max}	d'_{min}	I_{min}(mv)	I_{max}(mv)
41	.6767	.6620	346	361
42	.6914	.6767	361	377
43	.7061	.6914	377	393
44	.7208	.7061	393	410
45	.7355	.7208	410	427
46	.7502	.7355	427	444
47	.7649	.7502	444	461
48	.7796	.7649	461	479
49	.7943	.7796	479	498
50	.8090	.7943	498	516
51	.8237	.8090	516	535
52	.8384	.8237	535	554
53	.8531	.8384	554	574

TABLE 1. INTENSITY VERSUS SIZE

BIN NO.	d'_{max}	d'_{min}	I_{min}(mv)	I_{max}(mv)
1	.0886	.0739	4	6
2	.1034	.0887	6	8
3	.1181	.1034	8	11
4	.1328	.1181	11	14
5	.1475	.1328	14	17
6	.1622	.1475	17	21
7	.1769	.1622	21	25
8	.1916	.1769	25	29
9	.2063	.1916	29	34
10	.2210	.2063	34	39
11	.2357	.2210	39	44
12	.2504	.2357	44	49
13	.2651	.2504	49	55
14	.2798	.2651	55	62
15	.2945	.2798	62	68
16	.3092	.2945	68	75
17	.3239	.3092	75	83
18	.3386	.3239	83	90
19	.3533	.3386	90	98
20	.3680	.3533	98	107
21	.3827	.3680	107	116
22	.3974	.3827	116	125
23	.4121	.3974	125	134
24	.4268	.4121	134	143
25	.4415	.4268	143	154
26	.4562	.4415	154	164
27	.4709	.4562	164	175
28	.4856	.4709	175	186
29	.5003	.4856	186	197
30	.5150	.5003	197	209
31	.5297	.5150	209	221
32	.5444	.5297	221	234
33	.5591	.5444	234	247
34	.5738	.5591	247	260
35	.5885	.5738	260	273
36	.6032	.5885	273	287
37	.6179	.6032	287	301
38	.6326	.6179	301	316
39	.6473	.6326	316	330
40	.6620	.6473	330	346

beam and their scattered light can be inverted to size since the Gaussian ambiguity is removed. In Equation (4) the exponent can therefore be approximated as unity and we get

$$I_{S_2} = I_{O_2} K_2 G_2 \quad . \tag{5}$$

To obtain the particle diameter, d, it is necessary to know the functional relationship of K_2 (d,n,θ,Ω,λ,S) as given by Equation (12) of the 1984 annual report. The relationship between d and K_2 is programmed in a tabular form into a PROM in the computer interface. Table 1 shows the values contained in such PROM. There are 53 bins in the size histogram. These bins are defined by d'_{min} and d'_{max} which represent non-dimensional diameters: $d' = d/\delta CF$, where δ is the fringe spacing and CF a calibration factor. The last two columns show the minimum (I_{min}) and maximum (I_{max}) pedestal intensities of the corresponding bin.

3.1 Apparatus and Experimental Facility

Two different breadboards were designed and built to test the PIMAX technique. The first is a natural extension to the two-color IMAX breadboard used previously. A schematic of this breadboard is shown on Figure 1. A helium-neon laser provides the light source with wavelength of 6328 Å. A Wollaston prism splits the laser beam into two beams with S and P polarization. The intensity ratio of these two beams can be adjusted with a polarization rotator placed just before the Wollaston prism. One of these beams is then expanded with the use of lenses L_1 and L_2, which act as a beam expander, thus achieving the beam ratio

as it was shown in the 1984 annual report for spherical droplets much larger than the wavelength, K can be approximated by the laws of diffraction, refraction and reflection. Therefore, it is given by Equation (12) of the above report. Here it is assumed that the small beams have a polarization parallel to the scattering plane while the polarization of the big beam is perpendicular. G is the gain function of the instrument, and V is the visibility of the measured particle.

It should be pointed out that even though the visibility is a limited function to obtain the particle size it must be taken into account in any interferometric technique. The reason is that the visibility combined with the pedestal establish the ac modulation without which the particle would not be detectable. The size of the probe volume for a given particle size depends on its visibility. In simple terms the larger the visibility for a given pedestal, the larger the modulation and the larger the probe volume. Since the number of processed signals depend on the probe volume, the visibility must be reasonably well known. Note that the imposition of accuracy is less severe since an error in the visibility will not affect the size but it will affect , to a much less extent, the number of processed signals in any size class.

Equation (3) gives the signal response of the laser Doppler velocimeter which will establish the detectability of the signal. The processing logic will be the following: signals exhibiting ac modulation will have crossed the fringe pattern which is located in the middle of the large beam. Therefore, signals validated by the laser velocimeter correspond to particles crossing the middle of the large

$$I_1 = 2I_{o_1} \exp\left(\frac{-2}{b_{0_1}^2}\right)[x^2+y^2+z^2\gamma^2/4] \cdot \left[\cosh\left(\frac{2xz\gamma}{b_{0_1}^2}\right) + \cos\frac{4\pi x \sin\left(\frac{\gamma}{2}\right)}{\lambda}\right], \quad (1)$$

and

$$I_2 = I_{0_2} \exp\left[-\frac{2}{b_{0_2}^2}(x^2 + y^2)\right] \quad . \quad (2)$$

Where I_o is the center intensity, γ is the intersection angle, b_o the waist radius, λ the laser wavelength, and x,y,z the coordinates. The z dependence of the large beam is negligible. If we also assume that $\frac{zy}{2} = 0$ (which is an excellent assumption since a pinhole in the receiver will limit the value of z), the intensity scattered by a spherical particle is given by:

$$I_{s_1} = 2I_{0_1} K_1(d,n,\theta,\Omega,\lambda,P)G_1 \exp\left[\left(-\frac{2}{b_{0_1}^2}\right)(x^2+y^2)\right]\left[1 + \cos 2\frac{\pi\gamma x}{\lambda} \cdot V\right] , \quad (3)$$

and

$$I_{s_2} = I_{0_2} K_2(d,n,\theta,\Omega,\lambda,S)G_2 \exp\left[\left(-\frac{2}{b_{0_1}^2}\right)(x^2+y^2)\right] \quad , \quad (4)$$

where

K is the scattering cross-section. In general K is a complex function of size d, the index of refraction n, the collection angle θ, the solid angle of collection Ω, the wavelength λ and the polarization. However

4.0 EXPERIMENTAL RESULTS

4.1 Pre-Calibration Procedure

The calibration of the PIMAX relies very heavily on the accuracy of producing a reference size droplet. These droplets were produced with a Berglund-Liu generator, and their size could be predicted knowing the flow rate and droplet generation frequency. To test the accuracy of the Berglund-Liu generator the droplets were also photographed and their size obtained from a magnified negative. The droplets were measured with PIMAX before and after photographing them to insure consistency. The procedure for this experiment was to first produce a string of large monodisperse droplets to calibrate the PIMAX system. These large monodisperse droplets are normally formed by smaller, unstable droplets colliding into each other in the first 2 cm of the droplet string. Since the dispersion takes place at the orifice and the droplets are still in an unstable mode at that point, there can be no stable droplets in the dispersion spray for these large droplets.

Smaller droplets were then produced by increasing the frequency of the orifice vibration. These were stable and monodisperse at the point of inception and produced a well-behaved monodisperse spray with the aid of dispersion air which could then be measured with the calibrated PIMAX system.

The PIMAX system could not be calibrated on a string of small droplets directly, because there are always several droplets in the probe volume for the high frequency condition.

For the spray produced with the assistance of dispersion air the angle was about 10° and the number density typically 500/cm^3. The PIMAX

optical configuration consisted of a transmitting lens of 711 mm, small beam diameter of 80 μm, receiving angle of 20°, and receiving lenses of 300/495 mm.

The photographic system (Figure 4) consisted of a stroboscopic light source which illuminated a string of monodisperse droplets produced by a Berglund-Liu droplet generator. The scattered light from this string of droplets was collected by a 55 mm Olympus f 1.2 lens. The collected light was then relayed to a 490 mm lens which focused the image onto the film plane of an Olympus OM-2 body.

The Olympus camera was mounted on a rack and pinion rail for focusing. Since this was a constant magnification system, the movement of the camera did not affect the magnification of the droplets. The total system magnification from the droplet to the image on the film plane was approximately nine. A resolution chart (U.S.A.F. 1951) was also photographed with the same system and used as an absolute scale to calculate the droplet magnification. It also served to determine the resolution of the optical system. The smallest element of the last group (2.2 μm) was easily visible through the camera. The minimum resolution was obtained with the formula:

$$R = \sqrt{(1.22 \times \lambda \times F\ no.)^2 + \frac{Rf^2}{M}}$$

where λ is the wavelength of the strobe (assumed .5 μm for white light), F No. refers to the collecting lens which is 1.2, Rf is the resolution of the recording film of 3 μm, and M is the magnification ≈ 9. The minimum resolution is calculated to be .79 μm.

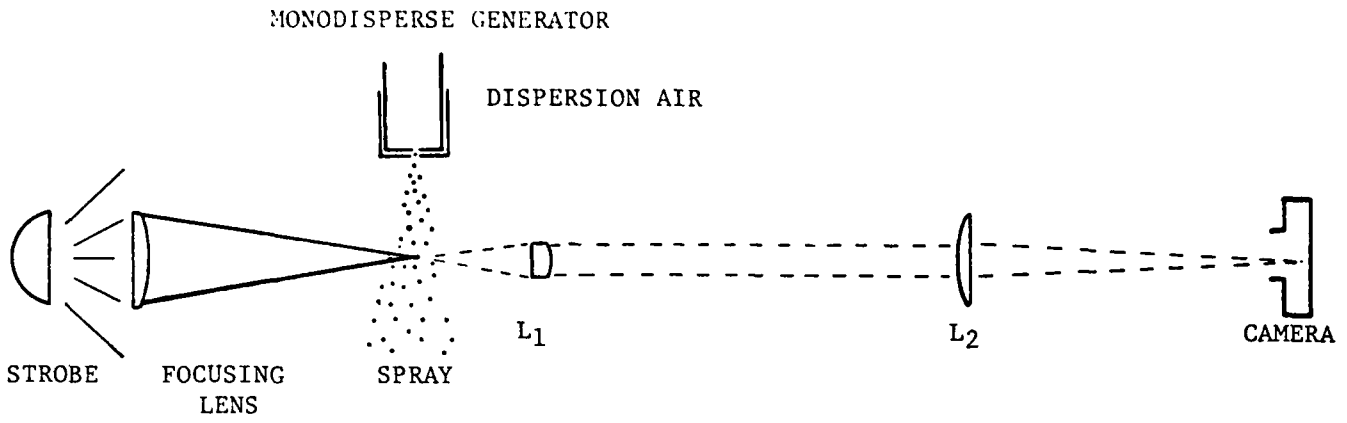

Figure 4. Schematic of Photographic system

Therefore, it was concluded that the resolution is less than 2.2 μm but larger than .8 μm due to noise in the system. The photograph of the resolution chart (Figure 5) shows a resolution of only 2.5 μm (7th group, 5th element). This is attributed to both the problem of the film lying flat at the plane of focus, and to a lesser degree, the resolution of the paper the negative was printed on.

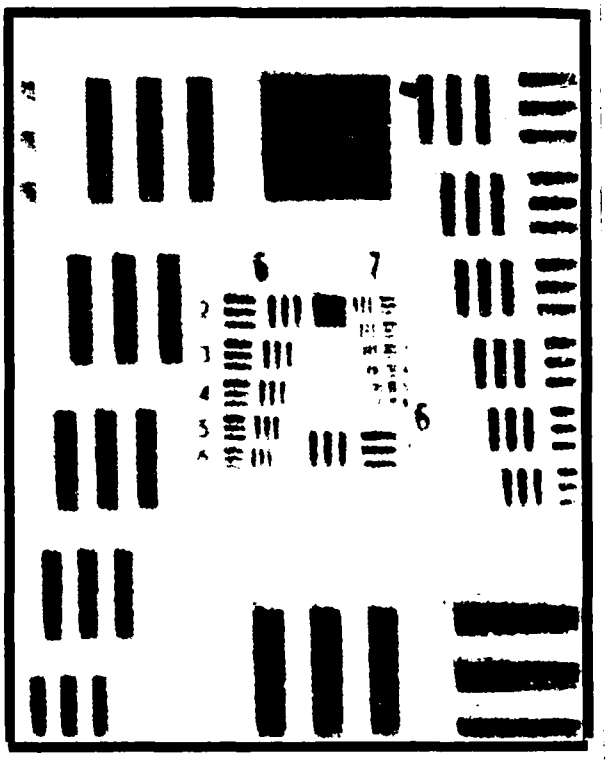

Figure 5. Photograph of resolution chart.

A Gen Rod 1539 stroboscope provided the source of illumination to the droplets for photography. It was used on its highest frequency setting, having a flash duration of 800 ns at 1/3 of the peak intensity. This exposure time was short enough to "freeze" the droplets which were traveling at about 6 to 10 m/s. The decay of the strobe flash left a faint "ghost image" of approximately 3 droplet diameters. The procedure for the flash photography was to open the shutter in a darkened room, remotely fire the stobe once, then close the shutter. An 8" focal length lens was used to focus the strobe light on the droplet stream to maximize illumination.

The film used was Kodak Technical Pan Film 2415 which is an extremely fine grain film (320 lines/mm). The film was given an exposure index of 50 and developed for 12 minutes at 75° in D-76 developer. This developing time was used to produce optimum optical density of .5, as measured on a densitometer, and a contrast index of 2.5.

The method of measurement was to place the negative in an enlarger and project it onto a white sheet of paper. The edges of both vertical and horizontal diameters were carefully marked and then those points measured through a 10x eyepiece with a reticle scale. The lengths of these diameters were averaged and then divided by the magnification factor of 132 which was obtained by measuring a negative of the resolution chart at the same magnification. The accuracy of measuring the droplets in this way is ± 1.5 μm. Two size droplets were photographed: an 80 μm droplet string produced with a flow rate of 0.3 cm^3/min and a frequency of 18.6 KHz, and a 52 μm produced with the same flow rate and a frequency of 69.4 KHz. The corresponding sizes obtained photographically are 78 μm and 50 μm. Figures 6a and 6b show the photo-

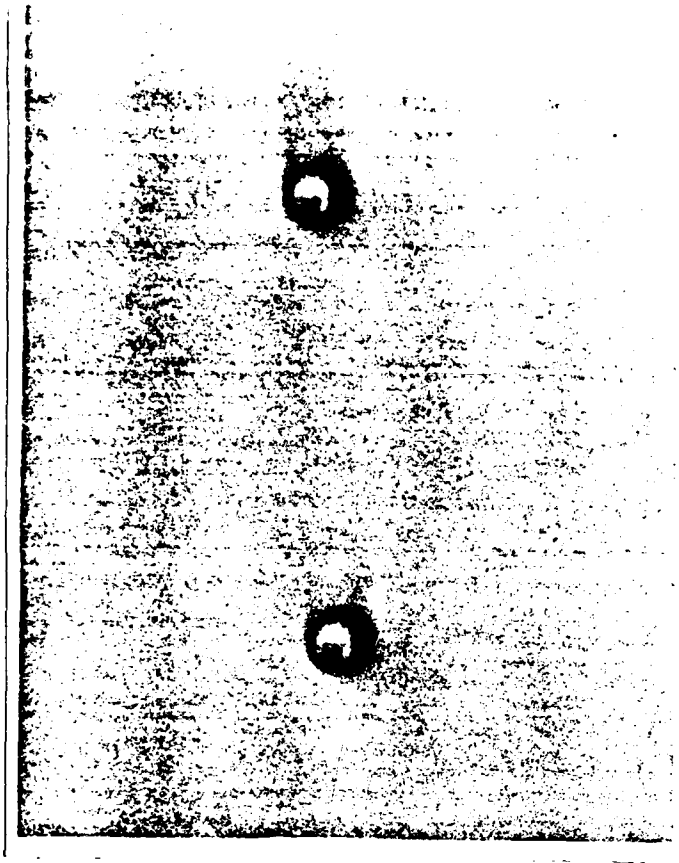

Figure 6a. Photograph of 80μm droplet string.

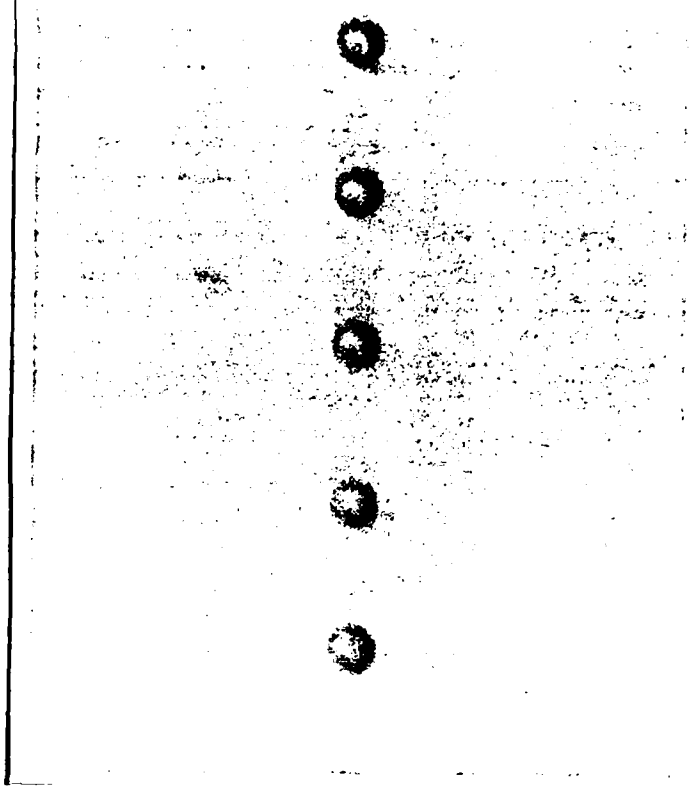

Figure 6b. Photograph of 52μm droplet string.

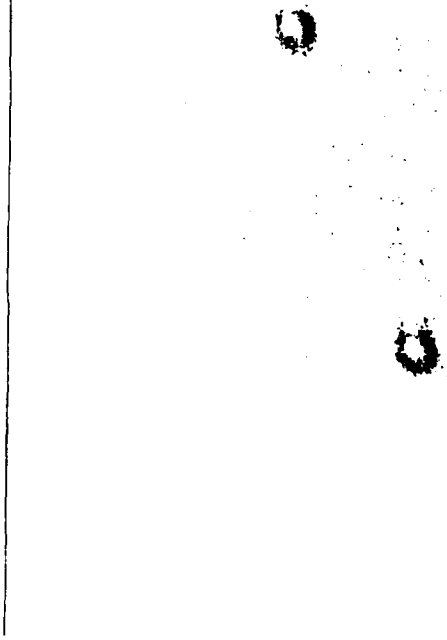

Figure 6c. Photograph of 52μm droplet spray.

graphs of the corresponding droplet strings. The 52 μm droplets were then dispersed with air to form a monodisperse spray. Here the photographic technique was more tedious since very few particles were in focus. Figure 6c shows a photograph of two of these droplets. The estimated size was also 50 μm. We could therefore conclude that the Berglund-Liu predicted size is photographically confirmed to 4% error.

The corresponding PIMAX histograms are shown on Figures 7a and 7b. The 81 μm size shown on Figure 7a is the calibration point obtained with a string of droplets. The spray of 52 μm droplets was then produced and the results shown on Figure 7b. Notice that the measured size was only 43 μm which implies that PIMAX under predicted the size by 20%. This error was repeatable and extremely consistent. It pointed out that there was a problem in the system which needed correction. We found that the problem was the result of using an 800 μm round pinhole on the BPMT which limited the ability to focus the image. In addition, BPMT was fixed, therefore, the alignment was performed prior to CP thus affecting both PMTs. Two corrective actions were taken. First the pinhole was substituted by a 150 μm x 3 mm slit, and the entire PMT assembly was mounted on traversing stages. Thus, the alignment of the large beam could be perfected after aligning the image to the SPMT.

After the above improvements were implemented, the system was used to acquire additional data following the same procedure as before: calibrate with 80 μm droplets, and measure smaller droplets in a string or spray mode. The results are shown below.

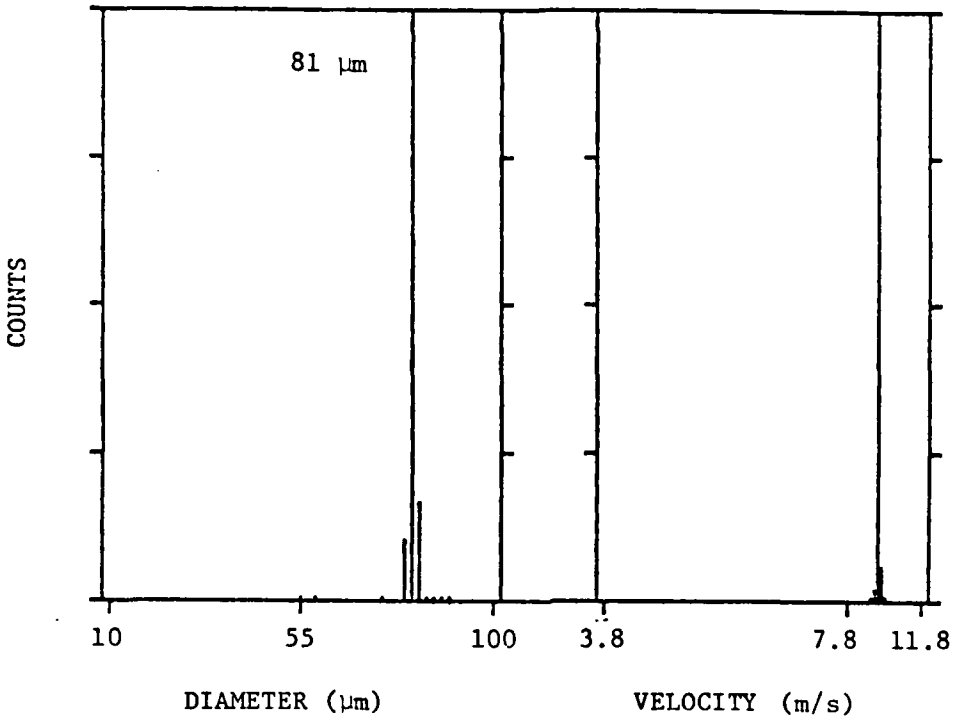

Figure 7a. Size and velocity histograms of a monodisperse string of droplets measured with PIMAX.

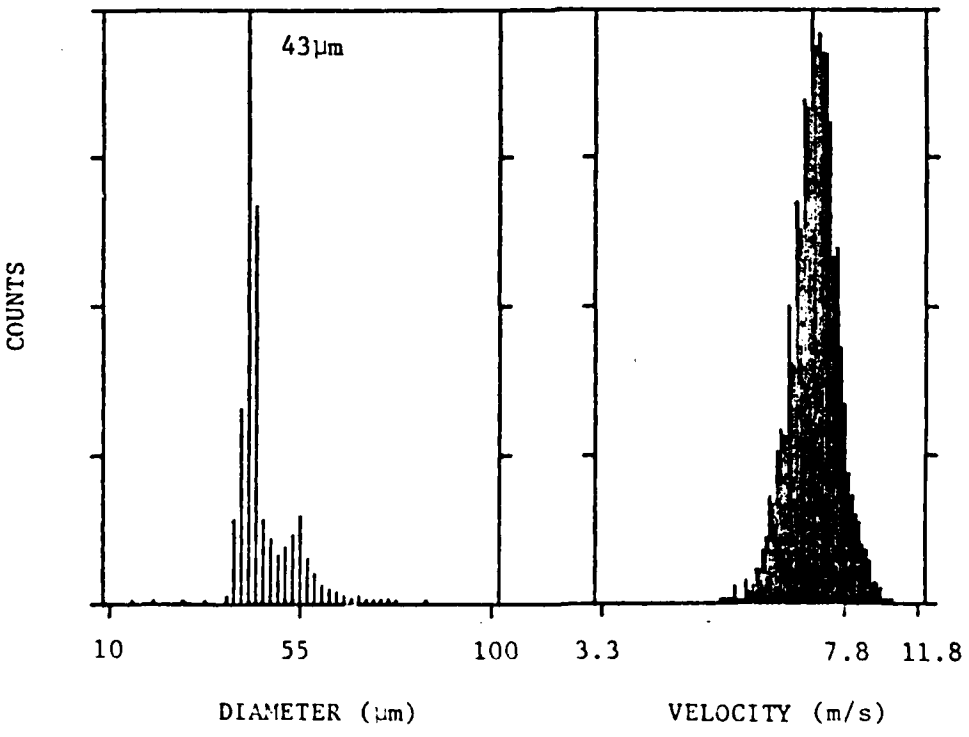

Figure 7b. Size and velocity histograms of a monodisperse spray (with some doublets) measured with PIMAX.

Droplets	Mode	$d_{predicted}$ (μm)	$d_{meas.}$ (μm)	error (%)	Series/Run
Monodisperse	String	59	60	+1.7	SLIT/14
	Spray	59	58	-1.7	/14S
	String	54	53	-1.9	/15
	Spray	54	53	-1.9	/15S
	String	52	51	-1.9	/23R
	Spray	52	49	-5.6	/23S

A look at the percent error column indicates that by introducing a slit in the big beam scattered light, the string of small droplets can now be measured and that a more accurate measurement of a spray of monodisperse droplets can be obtained. Typical errors achieved with these improvements done to the receiving optics are within 5%.

Typical histograms (size and velocity) for the monodisperse spray are shown on Figure 8. They correspond to the run SLIT/14S.

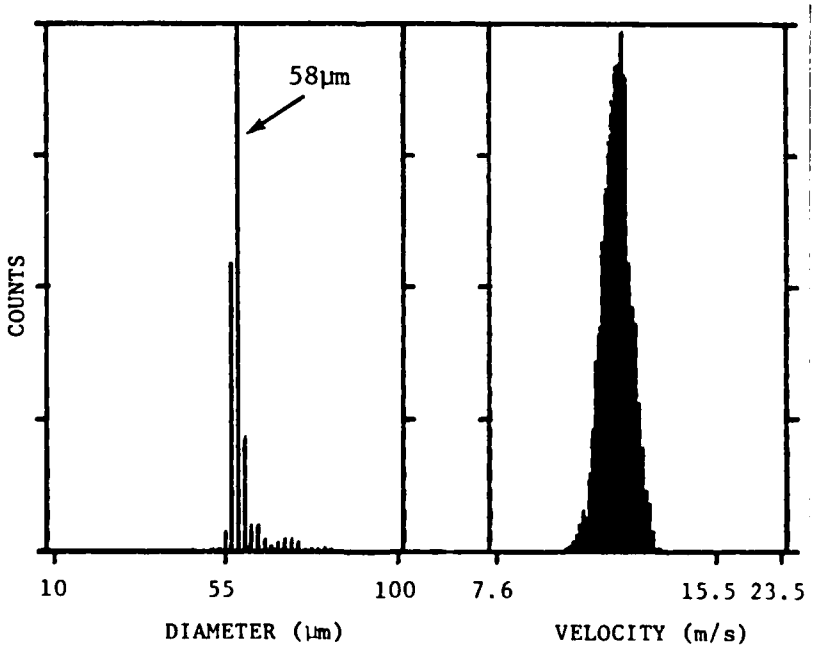

Figure 8. Size and Velocity histogram of a monodisperse spray of 58μm droplets.

4.2 Dynamic Size Range

The dynamic size range is defined as the ratio of maximum to minimum size measurable by a system with a given single configuration. The actual values of the extrema can change depending on the chosen configuration. For fuel sprays, as an example, the dynamic size range should be about 30:1. Therefore, an instrument with a narrower dynamic range would need two or more configuations to resolve the spray.

To establish the dynamic size range particles of various sizes should be measured and so should their signal to noise ratio. Thus, the minimum measurable size is established for a given upper limit.

In the present experiments the variety of sizes that could be generated was limited. Therefore, the approach taken was to simulate different size particles, given a stable droplet string. First, it is important to recognize that the scattered light signal is characterized by its amplitude and visibility. Both of these parameters were independently controlled during this experiment, primarily by masking the receiver and attenuating the laser beam. The S/N was estimated from the velocity histogram given that the stable droplet string produced a single velocity value. The signals of the simulated small particles had optical noise which was interpreted by the electronics as a broad velocity distribution. Using the velocity broadening as the criterion for signal acceptability, the maximum dynamic size range was estimated at 100:1 for a 25 mW He-Ne laser.

4.3 Spray Measurements Procedure

The procedure for acquiring spray data is presented here. This procedure starts with aligning the optical breadboard as shown in

Figure 2. The associated electronics are then checked and calibrated using a Berglund-Liu droplet generator. This calibration depends heavily on the stability of the droplet generator and its associated equipment as will be discussed. The final alignment of the receiver with respect to the transmitter is performed with steady stable signals appearing on the monitoring oscilloscope. The electronics are then calibrated to the known droplet size for the desired size range. Finally, the droplet generator is replaced by the spray nozzle and the measurements begin. A detailed discussion of the alignment procedure now follows. Upon completing a rough alignment of the transmitter, the probe volume is inspected by projecting it onto a screen with a 20X microscope objective lens. This allows careful adjustments of the transmitter before the droplet generator is in place. The droplet generator is then placed on an xyz traverse and a string of droplets is aimed at the center of the probe volume.

The light scattered from these droplets is collected by the receiving optics and imaged on two photomultipliers. The signals out of the PMTs are analyzed for amplitude, sharpness, symmetry, and visibility. The PMTs are mounted on traverse stages which allow very precise focus of the scattered light onto pinholes placed in front of them. A variable mask placed in front of SPMT permits the continuous change of the visibility associated with the produced droplet size. Notice that the calibration of the visibility is not critical since it is not used for sizing. However, the interferometric detection method requires the presence of ac modulation in the signal. Therefore, it is important that the visibility be nonzero for any particle in the measurement range.

The scattered light signals can also be used to fine tune the position of the polarization rotator to minimize crosstalk. Figure 9 shows an oscilloscope trace of signals corresponding to a well aligned system. The top tracer corresponds to the large beam while the bottom tracer coreresponds to the crossed small beams. The gains of the PMTs are then established to correspond to the measured droplet size. Notice that all the measurements are made relative to the calibration point. This calibration is not arbitrary for it must conform with the limitations of the electronics. Namely, the largest measurable particle must not saturate the electronics, and the smaller must be above the established threshold. Signals beyond these limits are ignored and would have to be measured with a different configuration.

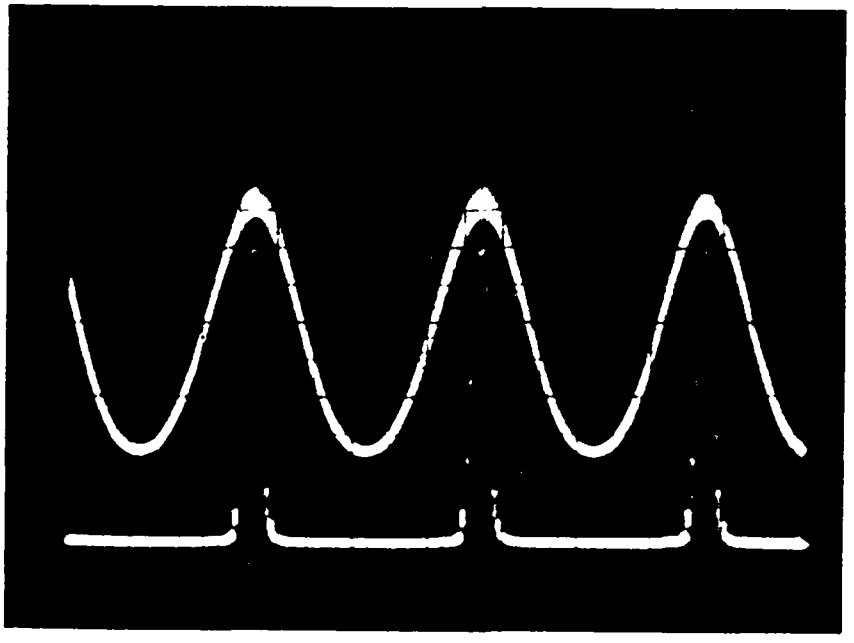

Figure 9. Oscilloscope trace of signals produced by a monodisperse string of droplets.

Upon completion of the alignment and calibration, the nozzle is located in place. The spray nozzle is mounted on a traverse stage to allow the measurement at different parts of the spray, as well as to permit very careful repetition of the nozzle position. A plumb ball hung from a fine string was attached to the tip of the nozzle. The nozzle was then traversed until the string intersected the optical probe volume. That position marked the (geometric) center of the spray. The nozzle was also oriented in the same way in every test. This was important since the spray proved to be nonsymmetrical. A pressure regulator controlled the water pressure to ensure the repeatability of the spray. Data were then acquired as a function of pressure and radial position. At the end of each day the nozzle was cleaned with ethyl alcohol and dried, with compressed Freon and lubricated with a few drops of fine oil. At the beginning of each day, the nozzle was cleaned with ethyl alcohol in an ultrasound bath.

4.4 Spray Results

A Parker-Hannifin simplex spray nozzle (Part No. 6730051M7) was characterized with the new PIMAX system. Three aspects of this work are described here. First, the effect of the probe volume correction in the size distribution is established. Two positions of the spray (the center and a radial position of 10 mm) were chosen for these studies. Second, the system's self-consistency is illustrated by acquiring and displaying the data in two overlapping size ranges (10 - 100 μm and 15 - 150 μm). Third, the spray is mapped as a function of radial position and pressure for an axial position of 50 mm.

Figures 10a and 10b show the raw counts and probe volume corrected counts of the size distribution of droplets in the center of the spray for a pressure of 50 psi. Both the raw and corrected counts are normalized by the time of collection and the size bin width. Notice that this latter is just proportional to the size range in question. The corrected counts are, in addition, normalized by the weighting function of the probe volume. Two key ideas are conveyed in these figures: First, probe volume correction is needed to unbias size distributions obtained with nonuniform intensity laser beams; second, broad size distribution can be resolved with a series of overlapping ranges. For instance, the size range of 10 - 150 μm is here resolved with the ranges 10 - 100 μm and 15 - 150 μm. Obviously, the ideal case would be to measure the broad size distribution with a single instrument range. It was shown earlier that with a 25 mw He-Ne laser PIMAX could resolve a size range of 30:1 given the proper electronics. In the meantime, however, these broad size ranges could be pieced together with several narrow ranges taking the probe volume correction into account.

It should be noted from Figures 10a and 10b that very little correction is required for the large diameters. This is not a general statement and it depends on the ac modulation (given by the product of the pedestal and the visibility) associated with any size droplet. In the reported experiments, we chose a size versus modulation dependence which would make the large droplets less subject to threshold variations. Nevertheless, there is a consistent error in the corrected counts of the large droplets, showing that the number of large droplets measured in the 10 - 100 μm size range is larger than the equivalent

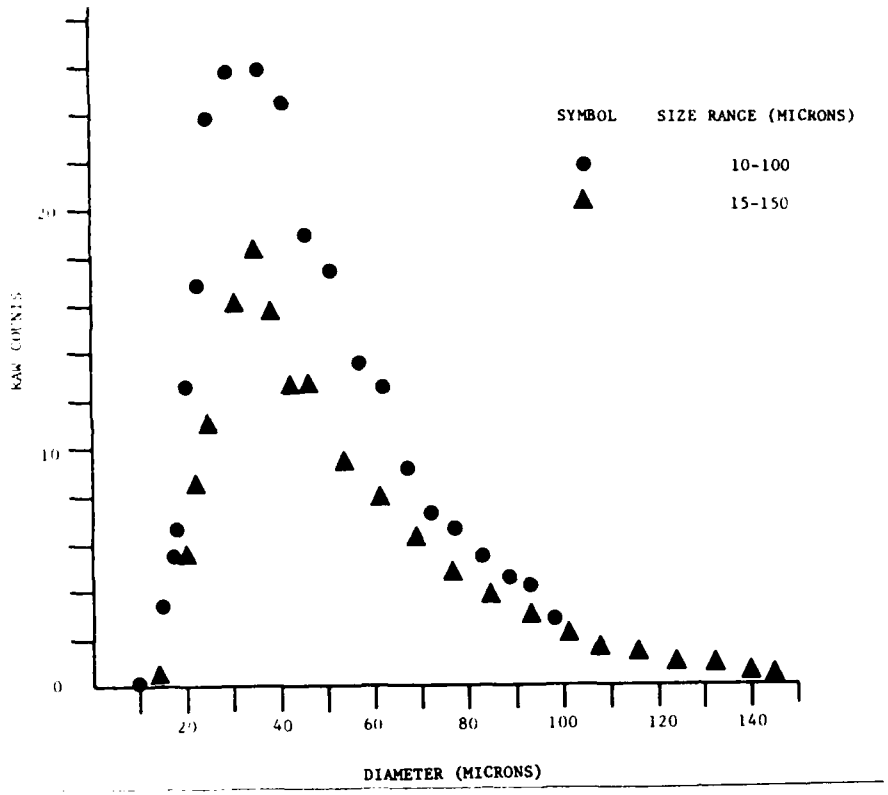

Figure 10a.

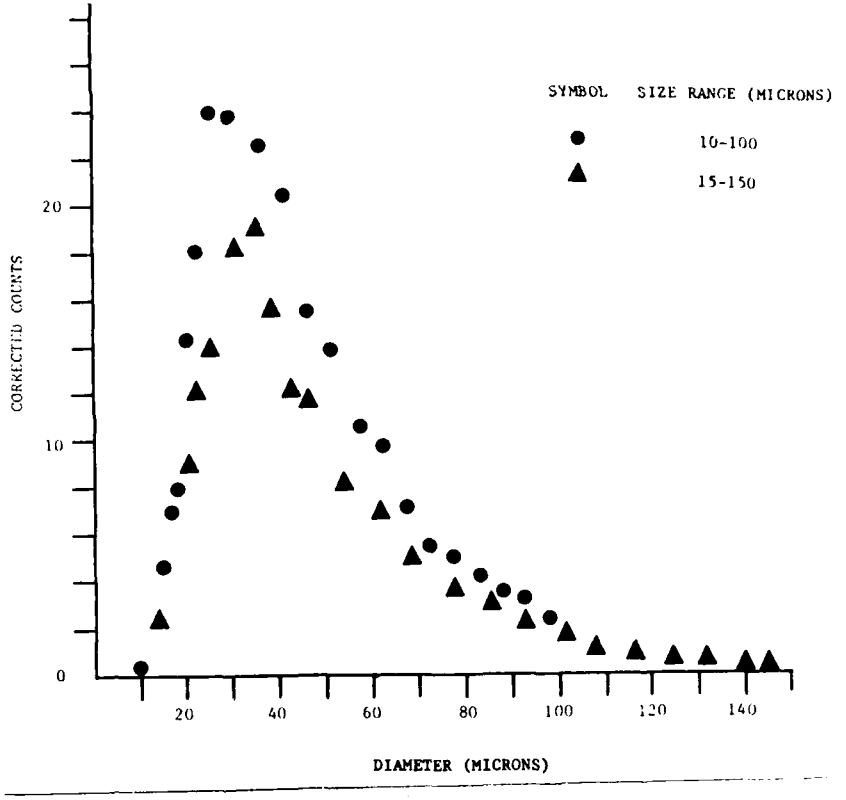

Figure 10b.

Figure 10. PIMAX measurements of a spray (produced by a Parker Hannifin nozzle No. 6730051M7 with water at 50psi) at a radial position of 0mm and axial position of 50mm: (a) uncorrected and (b) probe volume corrected.

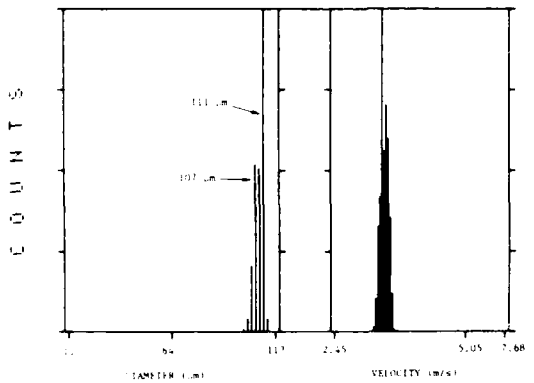

Fig. 7. I_{max} measurements of a string of monodisperse droplets.

ring of large monodisperse droplets to calibrate the strument. Smaller droplets were then produced by creasing the frequency of vibration of the orifice, and ith the dispersion air a spray of these droplets was rmed. The spray angle was ~10°, and the number ensity was typically 500/cm^3. The optical configuraon consisted of a transmitting lens of 711 mm, $m = 7$, ue waist diameter of 100 μm, receiving angle of 20°, id receiving lenses of 300/495 mm. The calibration oint was provided by a string of 110-μm droplets proiced with a flow rate of 0.21 cm^3/min and a frequency 5 kHz. Note that the droplet size can be precisely timated given the flow rate and number of equal oplets produced. Figure 7 shows the measured size id velocity. A spray of primary droplets of 49 μm roduced with a flow rate of 0.21 cm^3/min and freiency of 56.9 kHz) was then produced with the disersion air. Figure 8(a) shows the measurements of the ray of primary droplets. Figure 8(b) shows the easurements of a spray formed of primary droplets id doublets. The sizes predicted given the flow rate id frequency of droplet generation are 49 and 62 μm. he sizes measured with the NSPC were 46 and 57 μm, spectively. Figure 8(c) extends the measurements Fig. 8(b) to the presence of triplets. The predicted zes in this case are 49, 62, and 70 μm. Note that the

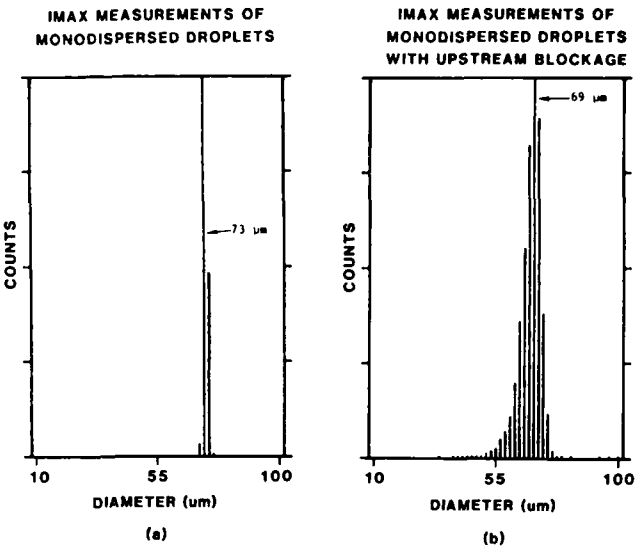

Fig. 9. Effect of beam blockage on size distribution.

diameters of the doublets and triplets measured with the NSPC are related to the primary droplets by $2^{1/3}$ and $3^{1/3}$, respectively.

X. Effect of Beam Blockage on Size Distribution

The effect of a spray blocking the laser beams before they cross on the size distribution measured with I_{max} was explored. A size range of 10–100 μm was used in this case, and the monodisperse droplet size was 73 μm.

Figure 9(a) shows the measurement of the monodisperse string of droplets. Figure 9(b) shows similar results, but a spray is blocking the laser beams. Two effects can be noted: the peak of the distribution dropped to 69 μm (5%), and the spread of the distribution is +5, −7 μm (+7, −10%) to the $1/e^2$. It should be noted that once the high voltage is corrected to account for the beam blockage, the broadening should have very little effect in the distribution of a polydispersed spray.

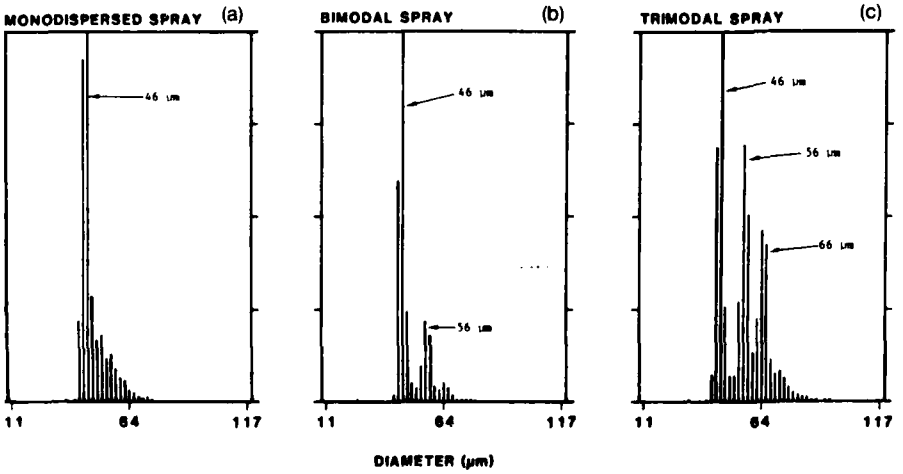

Fig. 8. I_{max} droplet size measurements.

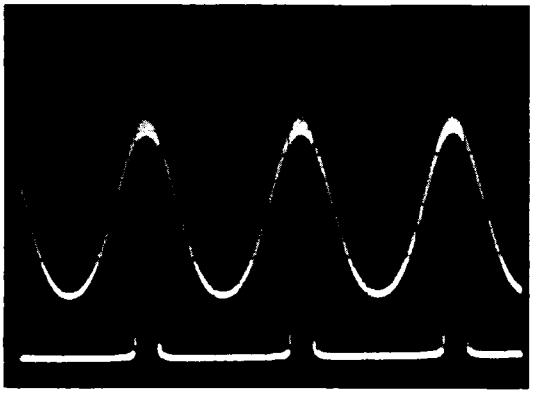

Fig. 5. Oscilloscope trace of signals produced by a monodisperse string of droplets.

period of sample i, and τ_0 is the processor's dead time after every sample.

The number density of size d is then given by

$$ND(d) = \frac{N(d)}{A(d)U(d)T}, \tag{25}$$

where $N(d)$ is the raw count of size d.

VIII. Description of Apparatus

An apparatus was designed and built based on the concepts presented earlier. In its simplest form this apparatus consists of (1) optics (transmitter and receiver), (2) electronic processor, (3) data management system (data handling and output devices).

Figure 4 shows a schematic diagram of a two-color breadboard optical system. An argon-ion laser provides the light source. The beam colors are separated by the dispersion prism, and two of these colors (the 5145 Å shown by the broken line and the 4880 Å shown by the solid line) are used to define the probe volume. A beam expander formed by lenses L_1 and L_2 define the beam ratio parameter m. A compensated beam splitter splits the blue beam into two beams, and the transmitting lens L_3 focuses and crosses these two blue beams in the middle of the green beam. The receiving optics use a dichroic mirror to separate the two colors of the scattered light. The probe volume is imaged on pinholes in front of two PMTs, and interference filters are used to perfectly separate the two colors. The outputs of the two PMTs are then inputs to the electronic processor. Figure 5 shows these outputs for a series of monodisperse droplets. This electronic processor consists of two major components: a frequency counter and a pulse height analyzer. The frequency counter uses the same principles as a LDV processor, and in this case it is a modified VP-1001 (SDL). The output of the blue PMT is the input to this processor. Its functions are to

(1) establish the threshold I_{min};
(2) measure the time of N fringes with $I_{ac} \geq I_{min}$;
(3) regulate the PMT high voltage; and
(4) bandpass the signal to reduce unwanted noise.

The output of the green PMT is input to the pulse height analyzer. As can be observed in Fig. 5, this signal has a simple Gaussian profile as given by Eq. (4). This pulse height analyzer is triggered by the frequency counter when signals exceed the threshold I_{min}. It measures the peak intensity of such a signal, and the validation is established in the frequency counter by measuring a preestablished number of fringes (typically twelve). Figure 6 shows a schematic representation of the processing logic.

The information of Doppler frequency and peak intensity is digitized, and two PROMs establish the bin numbers of a velocity and size histograms. A microprocessor based data management system accepts this information and handles the data. The data handling consists of real time display of the size and velocity histograms, data storage, analysis, and output (via printer or CRT). One of the programs to analyze the data computes the probe volume coordinate y as given by Eq. (23). This is used to correct the data by the probability of detection. Sample rates of several kilohertz are possible with this system.

IX. Results

A vibrating orifice droplet generator was used to produce strings and sprays of known size droplets. This generator produces a string of droplets of equal size and spacing. These droplets can be dispersed with external air to produce a spray of monodisperse droplets, or under some dispersion conditions the primary droplets will collide and form doublets and triplets.[11] The procedure used in these experiments was to produce a

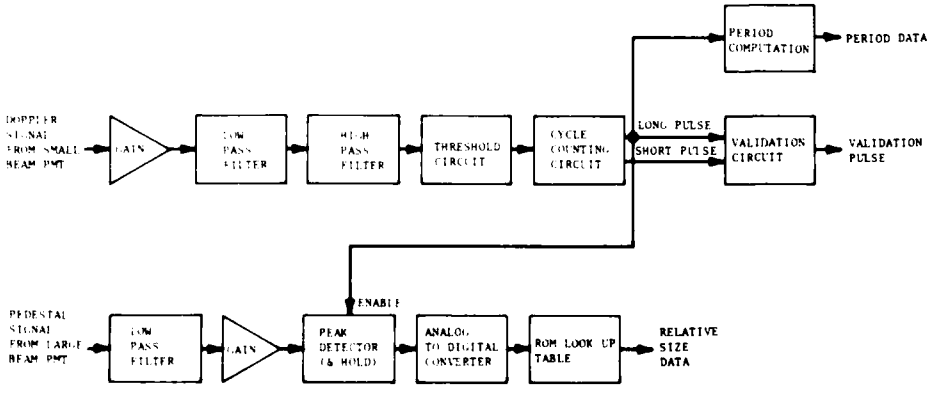

Fig. 6. Electronic block diagram of the droplet sizing two-color technique.

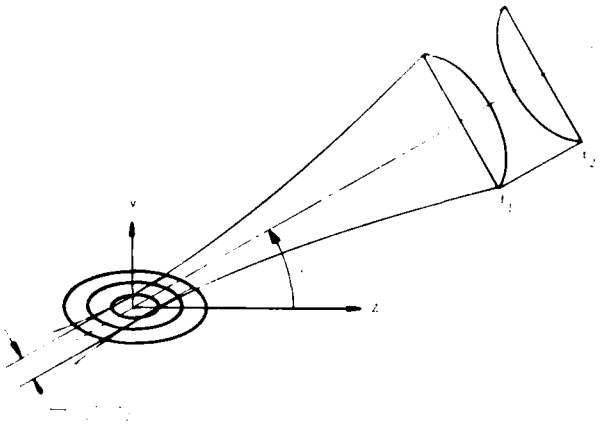

Fig. 3. Schematic representation of dual-beam probe volume limited by a pinhole.

over a larger region than those that scatter light with little modulation. As a result, the probe volume or region of detectability is a function of droplet size. Algorithms have been presented[10] to define the probe volume in LDV-type systems. A very simple algorithm will be presented here for the two-color system and off-axis collection.

Notice that only the small beams define the probe volume in this case, and, therefore, the probe volume will be a standard LDV-type volume. The approach followed will be very similar to the one described in Ref. 10.

There are two signal levels imposed by the electronics: the saturation I_{max} and the threshold I_{min}. The intensity to the peak of the ac modulation I_{peak} of the largest signal must be less than I_{max}, and the smallest detectable signal must be larger than I_{min} (defined peak-to-peak):

$$I_{peak_1} = 2I_{0_1}K_{0_1}d_0^2(1 + V_0) \leq I_{max}, \tag{20}$$

where d_0 produces the largest signal within the detectable size range, and V_0 is its corresponding visibility.

Solving for I_{0_1} we obtain

$$I_{0_1} = \frac{I_{max}}{2K_{0_1}d_0^2(1 + V_0)}. \tag{21}$$

This expression can now be substituted in Eq. (6) to obtain

$$I_{ac_1} = \frac{2d^2VI_{max}}{d_0^2(1 + V_0)} \exp\left[\left(-\frac{2}{b_{0_1}^2}\right)(x^2 + y^2)\right]. \tag{22}$$

and the detectability criterion establishes that $I_{ac_1} \geq I_{min}$ and that sufficient fringes are crossed. If we assume that the number of fringes processed by the electronics is equal to that in the waist diameter, $x = b_{0_1}$.

Solving for y in Eq. (22) we obtain

$$y \leq \sqrt{\frac{-b_{0_1}^2}{2} \ln\left[\frac{I_{min}}{2I_{max}}\left(\frac{d_0}{d}\right)^2 \frac{(1 + V_0)}{V}\right] - b_{0_1}^2}. \tag{23}$$

The cross-sectional area of sensitivity for an off-axis pinhole limited signal can be approximated by

$$A(d) = \frac{2D_p y}{\sin\theta} \cdot \frac{f_1}{f_2}, \tag{24}$$

where D_p is the pinhole diameter, and f_1/f_2 determines the magnification of the receiving optics. The effects of the pinhole and the coordinate system are illustrated on Fig. 3.

As seen by Eqs. (23) and (24) the area of detectability (in the y-z plane) is only a function of droplet size and corresponding visibility. This area can now be normalized and provide a weighting function to size distributions otherwise biased to the large signals.

This weighting factor is given by $w(d) = [A(d)]/A_{max}$.

The number density of any size droplet can also be calculated by dividing the number of counts of the given size by its corresponding sampling volume SV.

The sampling volume is a cylinder with cross section $A(d)$ and length equal to the droplet velocity $[U(d)]$ multiplied by the effective sampling time T, that is, $SV(d) = A(d)U(d)T$, and

$$T = TS - \sum_{i=1}^{M} N\tau D_i - M\tau_0,$$

where TS is the total sampling time to collect M samples, N is the number of fringes, τD_i is the Doppler

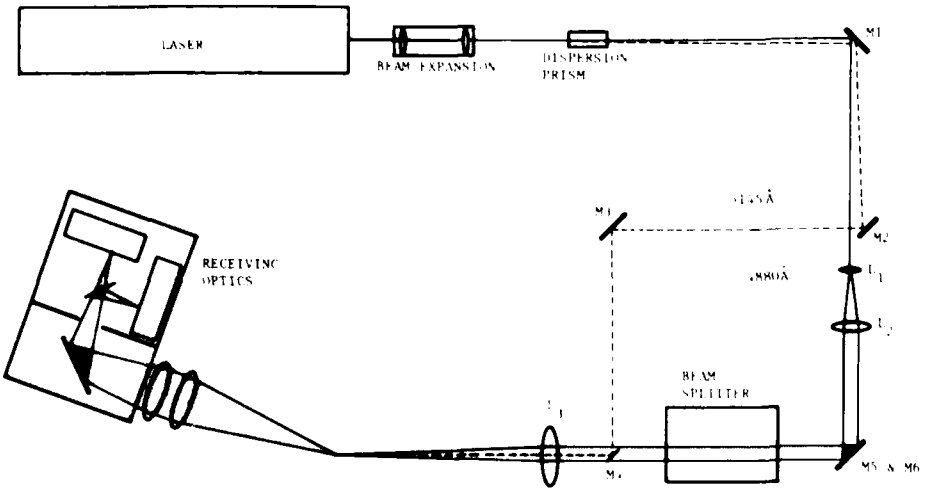

Fig. 4. Schematic I_{max} breadboard system.

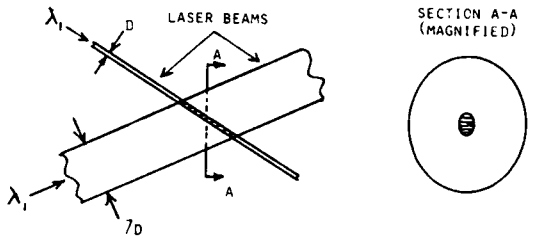

Fig. 2. Probe volume of single-color I_{max} technique.

system: (1) fringes are formed everywhere the large and small beams mix; (2) the pedestal of the large beam cannot be spectrally separated but electronically filtered. The intensity distribution of either beam can be expressed as

$$I_1 = I_{0_1} \exp\left[-\frac{2}{b_{0_1}^2}(x^2 + y^2)\right], \tag{11}$$

$$I_2 = I_{0_2} \exp\left[-\frac{2}{b_{0_2}^2}(x^2 + y^2)\right]. \tag{12}$$

The intensity scattered by the spherical particle can be expressed by

$$I_s = I_{s_1} + I_{s_2} + 2\sqrt{I_{s_1} I_{s_2}} \cos\beta \cdot V,$$

where $I_s = IK_0d^2$, and β is the phase angle; again it is assumed that the collecting lens is on the plane of symmetry of the two crossing beams. The pedestal is given by $P = I_{s_1} + I_{s_2}$ and the peak-to-peak ac intensity

$$I_{ac} = 2\sqrt{I_{s_1} I_{s_2}} V(\cos\beta = 1) - 2\sqrt{I_{s_1} I_{s_2}} V(\cos\beta = -1)$$
$$= 4\sqrt{I_{s_1} I_{s_2}} V,$$

that is,

$$P = I_{0_1} K_0 d^2 \exp\left[-\frac{2}{b_{0_1}^2}(x^2 + y^2)\right] + I_{0_2} K_0 d^2 \times \exp\left[-\frac{2}{b_{0_2}^2}(x^2 + y^2)\right], \tag{13}$$

$$I_{ac} = 4K_0\sqrt{I_{0_1} I_{0_2}} d^2 V \exp\left[-\frac{(x^2 + y^2)}{b_{0_1}^2} - \frac{(x^2 + y^2)}{b_{0_2}^2}\right], \tag{14}$$

following the same approach as before and again neglecting the contribution of diffraction for the off-axis collection angle. If we let $m = b_{0_2}/b_{0_1}$, we obtain

$$I_{ac_{min}} = 4K_0\sqrt{I_{0_1} I_{0_2}} d_{min}^2 \exp\left(-1 - \frac{1}{m^2}\right), \tag{15}$$

$$I_{ac_{max}} = 4K_0\sqrt{I_{0_1} I_{0_2}} d_0^2 V_0 \exp\left[-\frac{(b_{0_1}^2 + y^2)}{b_{0_1}^2} - \frac{(b_{0_1}^2 + y^2)}{m^2 b_{0_1}^2}\right]. \tag{16}$$

The variation in y will result in an error of the measured pedestal If we can assume that m is large, the pedestal of the large beam can be recovered by electronic filtering, and it is given by the second term of Eq. (13). This variation in y is obtained equating (15) and (16), and we obtain

$$y^2 = \frac{m^2 b_{0_1}^2}{m^2 + 1} \ln\left(\frac{d_0^2 V_0}{d_{min}^2}\right). \tag{17}$$

The error in the size will result from droplets crossing the pedestal of the large beam at $x = 0$ and y given by Eq. (17), that is,

Table II. Maximum Error in the Size Determination as a Function of Beam Ratio m and Measured Dynamic Size Range (d_{max}/d_{min})

m	d_{max}/d_{min}	$\frac{2y^2}{m^2 b_{0_1}^2}$	$\frac{I_{s_2}}{I_{0_2} K_{0_2} d^2}$	Max error (%)
7	10	0.113	0.89	5
7	20	0.168	0.84	8
7	30	0.2	0.2	10
5	10	0.22	0.80	10
5	20	0.32	0.72	15
5	30	0.39	0.68	18

$$\frac{I_{s_2}}{I_{0_2} K_0 d^2} = \exp\left(\frac{-2y^2}{m^2 b_{0_1}^2}\right). \tag{18}$$

Making similar assumptions as before $d_0 = 0.626 d_{max}$, $V_0 = 0.43$; therefore,

$$\frac{2y^2}{m^2 b_{0_1}^2} = \frac{2}{m^2 + 1} \ln\left[0.1685\left(\frac{d_{max}}{d_{min}}\right)^2\right]. \tag{19}$$

The maximum errors resulting from the finite size of the beams are presented in Table II.

It should be pointed out that the technique discussed here bases the detectability of the signal on the modulated or ac part of the scattered light. It is, therefore, important that no zeros are present in the visibility function. There are two other aspects of the theoretical foundation on which this technique is based which need to be taken into account. First, SPCs based on absolute scattered light require calibration at one datum point. This calibration can be difficult when measuring dense sprays, and a method to obtain automatic calibration is discussed. Second, provision must be made to account for the dependence of the probe volume as a function of particle size. These two algorithms will now be discussed.

IV. Self-calibrating Algorithm

The algorithm is based on measuring the visibility of any size class droplet. Combining the visibility and intensity[8] of the signal a very accurate measurement of the size can be made. Knowing the size of the chosen corresponding visibility one can establish the amplitude of the pedestal of this signal by adjusting the gain of the photodetector. The logic is as follows: for a given visibility (chosen in the most accurate region of the visibility function) there is an associated size and, therefore, an intensity scattered from the large beam. Since the intensity of this large beam is almost uniform, the scattered light associated with the chosen visibility will be almost constant in the absence of errors in the visibility. There are, however, errors associated with measuring visibility in a dense spray, and these points are rejected by V/I.[8] The process is an iterative one where V/I is implemented by choosing several narrow intensity bands to establish points out of control. The gain to the photodetector is adjusted until the majority of the points fall in the preestablished intensity band corresponding to the measured size.

VII. Probe Volume

The dynamic range exercise indicated that droplets that scatter light with large modulation are detectable

plane of symmetry of the crossing beams. The above equations show that the scattered light intensity is proportional to the square of the diameter of the sphere. This approximation is only valid for diameters larger than ~10 wavelengths. Note that the angle θ (deviation of incident pencil of light) to an arbitrary position of the lens is different for both beams (except on the line of symmetry). However, the integrated value is the same as long as the collecting lens is in the plane of symmetry. In this technique the ac modulation of I_{s_1} is used to establish detectability of the signal and to measure velocity. For a given threshold level (minimum ac signal accepted by the electronics), the larger the dynamic size range, the farther from the center of the beam the largest particle can cross and still exhibit ac modulation and, therefore, be detectable. This will introduce an error in the measurement as will be discussed in the next section.

The peak-to-peak ac signal is then given by

$$I_{ac_1} = 4I_{0_1}K_{0_1}Vd^2 \exp\left[\left(-\frac{2}{b_{0_1}^2}\right)(x^2+y^2)\right], \quad (6)$$

and the pedestal is given by

$$P_1 = 2I_{0_1}K_{0_1}d^2 \exp\left[\left(-\frac{2}{b_{0_1}^2}\right)(x^2+y^2)\right]. \quad (7)$$

Note that the pedestal is simply the sum of the Gaussian intensities without interference.

IV. Dynamic Size Range and Error Analysis

There are two known sources of error in the IMAX method. First is the error introduced by beam blockage produced by other particles in the trajectory of the beams and scattered light. This one is difficult to quantify and will be discussed with the results. Second, since the small beam has a finite diameter, the particles can travel a small distance away from the center of the big beam and still cross sufficient fringes to be detectable. The farther from the center it can be detectable, the larger the error it can produce. It will be shown here that this error increases with dynamic size range and decreases with the ratio of the large to small beam.

The dynamic range is limited by the electronic and optical noise. In general, we can establish that there is a threshold associated with the minimum processable ac signal and a saturation level associated with the largest signal processible by the electronics. All the signals accepted by the electronics must fall between these two limits. Equation (6) gives the peak-to-peak ac signal. Notice that both the diameter d and the visibility V influence the above expression.

To simplify this analysis we will neglect the contribution of diffraction at a collection angle of 30°. This assumption is reasonable for spheres larger than 7 μm where the contributions of reflection and diffraction are < 16%. The dynamic range is actually larger when diffraction is included.

The minimum processible ac signal is produced by the smallest particle (with diameter d_{min}) crossing the probe volume at $y = 0$ and crossing the minimum number of fringes required by the electronics ($x = b_{0_1}$).

Therefore, $I_{ac_{min}} = 4I_{0_1}K_{0_1}d_{min}^2 \exp(-2)$, where it has been assumed that the visibility of the smallest particle is 1.

The maximum ac signal is produced by a droplet of diameter d_0 (not necessarily d_{max}) and visibility V_0:

$$I_{ac_{max}} = 4I_{0_1}K_{0_1}d_0^2V_0 \exp\left[\left(-\frac{2}{b_{0_1}^2}\right)(x^2+y^2)\right]. \quad (8)$$

The farthest from the center this particle can be detected is when $I_{ac_{max}} = I_{ac_{min}}$, and it crosses a sufficient number of fringes ($x = b_{0_1}$). Therefore,

$$4I_{0_1}K_{0_1}d_0^2 \exp\left[\left(-\frac{2}{b_{0_1}^2}\right)(b_{0_1}^2+y^2)\right] = 4I_{0_1}K_{0_1}d_{min}^2 \exp(-2).$$

Solving for the size range, we obtain

$$\left(\frac{d_0}{d_{min}}\right)^2 = \frac{\exp(-2)}{V_0}\exp\left[\frac{2(b_{0_1}^2+y^2)}{b_{0_1}^2}\right] = \frac{1}{V_0}\exp\left(\frac{2y^2}{b_{0_1}^2}\right),$$

$$2y^2 = b_{0_1}^2 \ln\left[\left(\frac{d_0}{d_{min}}\right)^2 \frac{V_0}{\exp(-2)}\right] - 2b_{0_1}^2,$$

which results in

$$2y^2 = b_{0_1}^2 \ln\left[V_0\left(\frac{d_0}{d_{min}}\right)^2\right]. \quad (9)$$

The error in the size will be due to an error in the intensity scattered by the large beam when the particle crosses at $y > 0$ (notice that the particle must cross through $x = 0$). If we state that the large beam is m times larger than the small one,

$$\frac{I_{s_2}}{I_{0_2}K_{0_2}d^2} = \exp\left(\frac{-2y^2}{m^2b_{0_1}^2}\right). \quad (10)$$

To simplify the error analysis, let us assume that the optical parameters are chosen so that for any size range the visibility of the largest droplet is larger than zero.

Then the maximum ac signal is produced by a particle of diameter $d_0 = 0.626d_{max}$, and its visibility is 43%.

Substituting these values into Eq. (9), we obtain

$$\frac{2y^2}{b_{0_1}^2} = \ln\left[0.1685\left(\frac{d_{max}}{d_{min}}\right)^2\right].$$

The maximum errors resulting from the finite size of the beams are presented in Table I.

Table I. Maximum Error in the Size Determination as a Function of Beam Ratio m and Measured Dynamic Size Range (d_{max}/d_{min})

m	d_{max}/d_{min}	$\frac{2y^2}{b_{0_1}^2}$	$\frac{I_{s_2}}{I_{0_2}K_{0_2}^2}$	Max error (%)
7	10	2.82	0.94	3
7	20	4.21	0.92	4
7	30	5.02	0.90	5
5	10	2.82	0.89	5
5	20	4.21	0.85	8
5	30	5.02	0.82	10

V. Single-Color System

Figure 2 shows a schematic representation of the probe volume formed by crossing two beams of the same wavelength but different diameters. There are several fundamental differences between this and the two-color

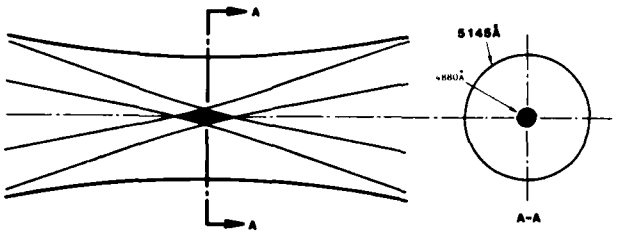

Fig. 1. Probe volume of two-color I_{max} technique.

(3) Visibility alone cannot be used to calibrate attenuation, since the very attenuation reduces the fringe visibility and randomly modifies the phase of the beams. Instead a combination of visibility and intensity is used[8] to establish the validity of the signal and calibrate the attenuation.

The mathematical model presented here is for spherical particles much larger than the wavelength, and we use diffraction, refraction, and reflection to characterize the scattered light.[9] This results in closed form solutions of the dynamic range and error.

Results are presented for sprays of known characteristics.

II. Problem Statement

The method discussed here bases the size measurement on the absolute intensity scattered by the droplet crossing the probe volume and the velocity measurement on the classical Doppler signal. It is referred to as the IMAX method. *In situ* single-particle counters are limited because of the nonuniform profile (typically Gaussian) of laser beams. Under this condition a particle crossing the middle of the beam will scatter more light than a similar particle crossing through the edge. Therefore, the relationship between size and scattered light is not unique.

To circumvent this problem, two beams of unequal size are crossed so that the small beam identifies the middle of the large beam and, therefore, removing the Gaussian ambiguity. Laser beams are chosen because of their spatial and temporal coherence and because of their size. These beams will interfere where they cross, and a fringe pattern will be formed in the middle of the large beam. Signals exhibiting an ac modulation will have crossed the fringe pattern and, therefore, the middle of the large beam. Both size and velocity of individual spherical particles can be extracted from this signal.

At least two approaches can be used to implement the above concept. The first consists of crossing two laser beams of different diameters but with the same wavelength. In the second two small beams of one wavelength cross in the middle of a larger beam of another wavelength. These approaches will now be explained starting with the second.

III. Two-Color System

Figure 1 illustrates the probe volume of this method. A spherical particle crossing through the fringes will also cross through a region of almost uniform intensity of the large beam. The ratio of the two beam diameters will establish the uniformity of the intensity incident on the droplet.

If we refer to the small beam as 1 and the large beam as 2, the intensity profiles in the probe volume can be spectrally separated and given by

$$I_1 = 2I_{0_1} \exp\left[\left(\frac{-2}{b_{0_1}^2}\right)(x^2 + y^2 + z^2\gamma^2/4)\right] \cdot \left[\cosh\left(\frac{2xz\gamma}{b_{0_1}^2}\right) + \cos\frac{4\pi x \sin(\gamma/2)}{\lambda}\right], \quad (1)$$

$$I_2 = I_{0_2} \exp\left[-\frac{2}{b_{0_2}^2}(x^2 + y^2)\right], \quad (2)$$

where I_0 is the center intensity, γ is the intersection angle, b_0 is the waist radius, λ is the laser wavelength, and x,y,z are the coordinates. The z dependence of the large beam is negligible. If we also assume that $(z\gamma)/2 \approx 0$ (which is an excellent assumption since a pinhole in the receiver will limit the value of z), the intensity scattered by a spherical particle is given by

$$I_{s_1} = 2I_{0_1}K_{0_1}d^2 \exp\left[\left(-\frac{2}{b_{0_1}^2}\right)(x^2 + y^2)\right]\left(1 + \cos 2\frac{\pi\gamma x}{\lambda} \cdot V\right), \quad (3)$$

$$I_{s_2} = I_{0_2}K_{0_2}d^2 \exp\left[\left(-\frac{2}{b_{0_2}^2}\right)(x^2 + y^2)\right], \quad (4)$$

where

$$K_0 = \frac{1}{4r^2}\int_{A_{lens}}\left\{[\varepsilon^2(\theta,n)D(\theta)]_{refraction} + [\varepsilon^2(\theta,n)D(\theta)]_{reflection} + \left[\frac{J_1^2(\alpha\sin\theta)}{\sin^2\theta}\right]_{diff}\right\} dA. \quad (5)$$

K_0 is a scattering coefficient, D is the divergence, n is the index of refraction, ε is the fraction of energy for every ray reflected or refracted, d is the diameter of a spherical particle, V is its visibility (defined as the ratio of the modulated signal to the pedestal), r is the distance from the scattering center to the collecting lens, and θ is the collection angle measured from the forward direction. It can be shown[9] that the contributions of these three terms are a function of angle. To keep the following analysis simple we will choose a collection angle θ of 30°. Assuming that the solid angle of the collecting lens is small with respect to θ, we can compare the intensities scattered at the discrete angle θ.

The refraction or reflection terms are given by $i_R = \alpha^2\varepsilon^2D$ and the diffraction by

$$i_D = \frac{\alpha^2}{\sin^2\theta}J_1^2(\alpha\sin\theta),$$

where $\alpha = (\pi d)/\lambda$ is the size parameter, and J_1 is the Bessel function of the first kind. Reference 9 shows that for S polarization

$$i(\text{refraction}) = 1.0375\alpha^2,$$

$$i(\text{reflection}) = 0.0785\alpha^2,$$

and it can be calculated that $i_D(\alpha) \leq 0.088\alpha^2$ for $\alpha \geq 49$ ($d \geq 7.6\ \mu m$).

At this angle the combined reflected and diffracted light represent 16% of the refracted light, which implies that in general the three components must be taken into account. It is assumed that the collecting lens is in the

Reprinted from Applied Optics, Vol. 23, page 4375, December 1, 1984

Nonintrusive optical single-particle counter for measuring the size and velocity of droplets in a spray

Cecil F. Hess

A technique for measuring nonintrusively, and in real time, the size and velocity of droplets in a spray is presented. A small beam identifies the center of a larger beam, thus defining a region of almost uniform intensity, and only droplets crossing through such a center are measured. The size is obtained from the absolute scattered light and the velocity from the modulated signal produced by the interferometric pattern. A self-calibrating algorithm is also discussed. Results are presented for a spray of predictable characteristics.

I. Introduction

A novel nonintrusive single-particle counter (NSPC) to measure the size and velocity of particles in a two-phase flow is described here. This method bases the size information on the absolute light scattered by individual particles crossing through the middle of a Gaussian laser beam. To define the middle of the Gaussian profile, two laser beams of different diameters are crossed so that the small beam intersects the middle of the large beam. Thus an interference pattern of fringes is formed in the crossover, defining a region of almost uniform intensity in the large beam. Both size and velocity information can be obtained from signals exhibiting adequate Doppler modulation. An alternative method consists of crossing two small beams of a given wavelength in the middle of a large beam of a different wavelength. NSPCs find application in many areas where the spatial resolution of size and velocity distributions is needed, for example, fuel spray studies, aerosol studies, flue gas desulfurization, spray drying, paint sprays, and sizing biological structures. They are also very useful on in-line monitoring and quality control systems where no extraction of samples is desired.

Several NSPCs using absolute scattered light have been proposed, and they can be divided into two groups. In the first group[1-3] Gaussian laser beams are used, and various mathematical inversion techniques have been proposed to extract the true size distribution from the signal amplitude distribution. Several assumptions are needed to perform such inversion, such as assuming the form of the size distribution[1] or a uniform average velocity for all the particles regardless of size.[2]

A method to account for the loss of collected light due to particles partially masked by a pinhole has also been described.[3] The second group of NSPCs uses a probe volume of known illumination to avoid the ambiguity of particle position. The technique described here falls in this group. Several approaches have been proposed[4-7] to accomplish this task. Apertures are used to cut off the edges of the Gaussian beam and thus image a probe volume of almost uniform illumination.[4,5] One of the apertures[4] had, in addition, two wedges that when properly oriented can be used to obtain the velocity vector in two components (magnitude and direction). Ring-shaped probe volumes have also been produced[6] by a TEM_{01} laser and a ring-shaped aperture. The measurement volume is defined by the intersection of apertures in front of two photomultipliers. A method[7] very similar to the two-color method described here which evolved independently has also been used. Four beams of two different colors are crossed forming two fringe patterns of different size so that the small fringe pattern is in the middle of the large one. To extend the dynamic range of the visibility technique, they used visibility to cover part of the size range and intensity to cover the rest. The term visibility refers to the ratio of the modulated part of the signal to the pedestal of a Doppler signal.

Some of the differences between the latter method[7] and the one reported here are as follows:

(1) The technique reported here is based on a single color, and the two-color system uses three beams instead of four.

(2) Visibility is not used to obtain part of the size distribution.

The author is with Spectron Development Laboratories, Inc., 3303 Harbor Boulevard, Costa Mesa, California 92626.

Received 18 Nov. 1983.
0003-6935/84/234375-08$02.00/0.

APPENDIX A

6.0 PROFESSIONAL PERSONNEL

Cecil F. Hess, Ph.D.	Principal Investigator
Donn Silberman	Research Engineer
Victor Espinosa	Research Engineer

5.0 PUBLICATIONS

1. Hess, C. F., "A Technique Combining the Visibility of a Doppler Signal with the Peak Intensity of the Pedestal to Measure the Size and Velocity of Droplets in a Spray," AIAA Paper Number 84-0203, presented at AIAA 22nd Aerospace Sciences Meeting, January 9-12, 1984, Reno, Nevada.

2. Hess, C. F. and Espinosa, V. E., "Spray Characterization with a Nonintrusive Technique Using Absolute Scattered Light," Optical Engineering, Vol. 23, No. 5 (1984).

3. Hess, C. F., "Nonintrusive Optical Single-Particle Counter for Measuring the Size and Velocity of Droplets in a Spray," Applied Optics, Vol. 23, No. 23 (1984).

Publications in Progress

1. Hess, C. F., "An Instrument to Measure the Size and Velocity of Particles in Particle Laden Flows," submitted for presentation at the AIAA/SAE/ASME 21st Joint Propulsion Conference, Monterey, CA, July 8-10, 1985.

symmetrical. Figure 12b shows the variation of SMD as a function of radial position for the same two pressures. As can be observed, there is a distinct difference in SMD for the two pressures. In addition, there is some dependence of the SMD in the radial position.

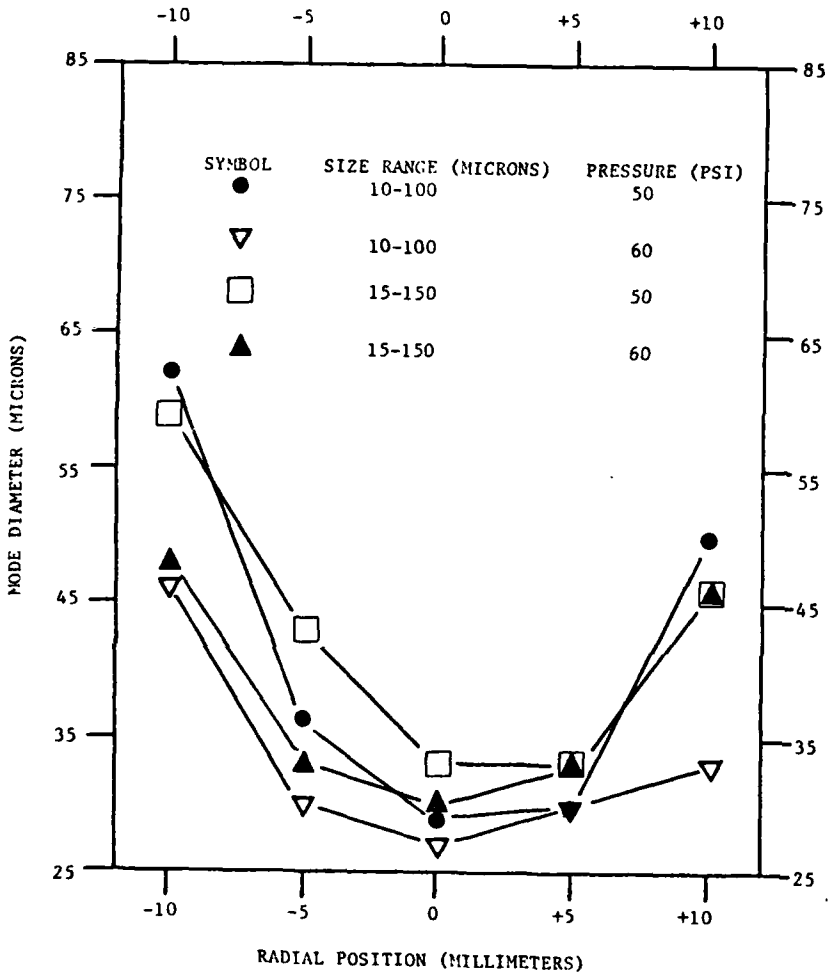

Figure 12a.

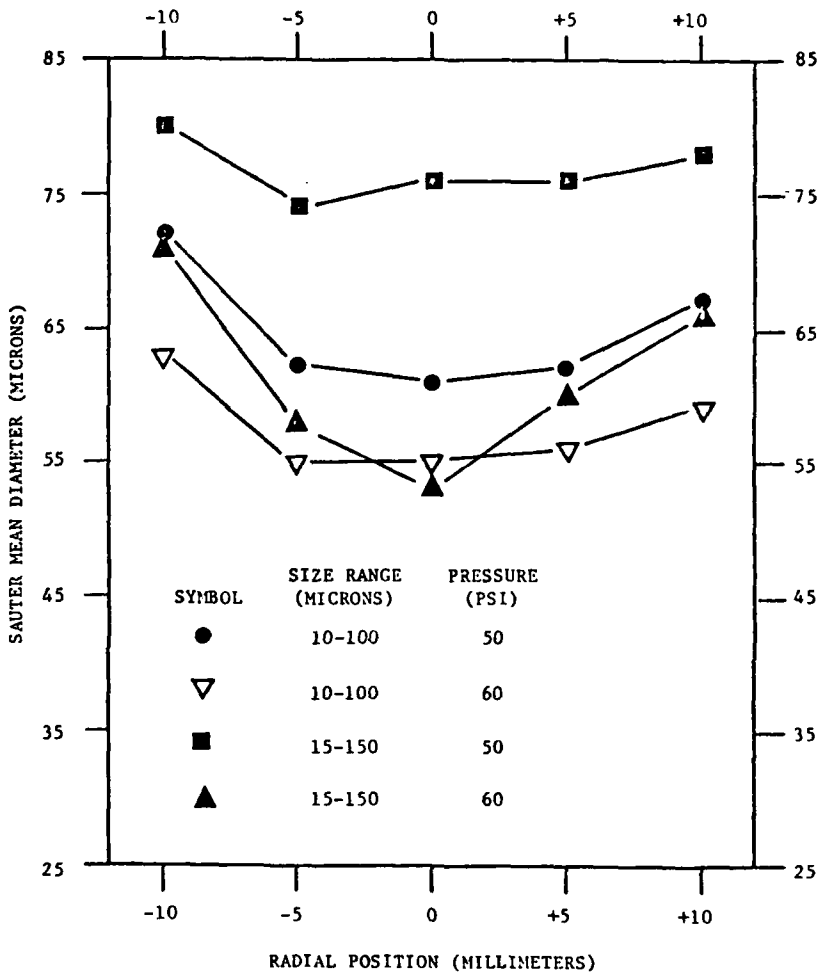

Figure 12b.

Figure 12. Variation of characteristic diameter of spray with radial position and pressure: (a) peak diameter; (b) Sauter mean diameter.

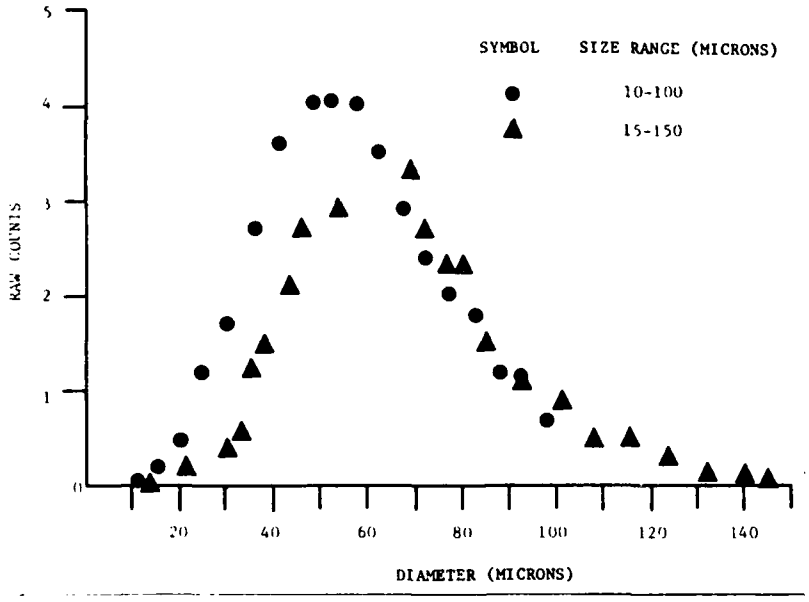

Figure 11a.

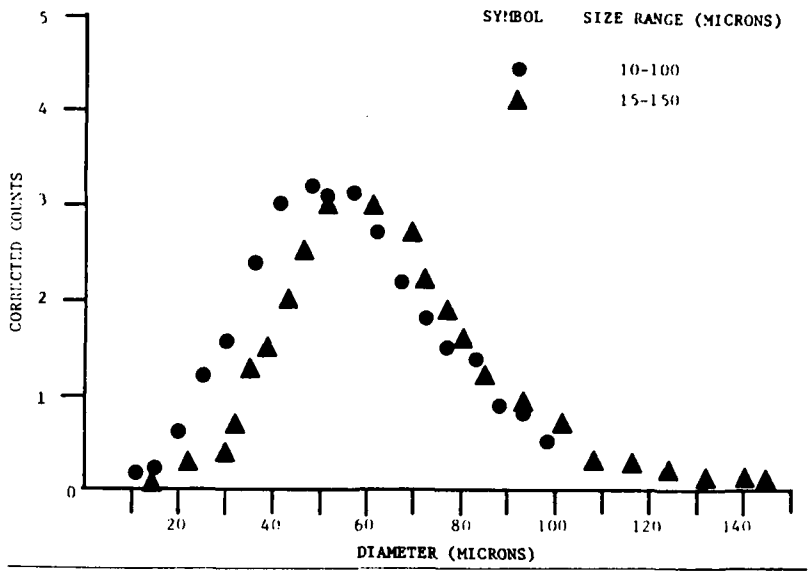

Figure 11b.

Figure 11. PIMAX measurements of a spray (produced by a Parker Hannifin nozzle No. 6730051M7 with water at 50psi) at a radial position of 10mm and axial position of 50mm: (a) uncorrected and (b) probe volume corrected.

measurement in the 15 - 150 μm range. This was not an isolated case limited to the reported data but was very consistent and reproducible. We conducted probe volume parametric studies to estimate the effect of having errors in the threshold, visibility, saturation level and number of fringes. These studies showed that only very gross errors in the above parameters would account for these variations in the number of counts. It is more feasible to expect that the instrument sensitivity differs from the theoretical one, either because of some nonlinear effect in the electronics or optics, or due to an error in our procedure. The size distributions obtained with the two ranges are, however, very similar, and the effect of the probe volume is very noticeable in the small size end. Raw and corrected data are also shown on Figures 11a and 11b corresponding to a radial position of 10 mm and the same pressure (50 psi) and axial position (50 mm) as before. Here, there is less discrepancy in the counts of the large droplets and more in the small droplets. The trend in the size distribution is the same that was reported before. Namely, there are more small particles in the middle of the spray than at the edge.

Size and velocity distributions were obtained at five radial positions and the results are shown on Figures 12a and b. The first shows the variation of peak diameter at 50 psi and 60 psi. As can be observed, the peak of the distribution changes almost a factor of 2 between a radial position of zero and -10 mm. It can also be observed by comparing the data of -10 mm with that of +10 mm that the spray is not

XI. Conclusions

This paper demonstrates the feasibility of using Gaussian laser beams to perform droplet size measurements using the absolute intensity of the scattered light. This concept extends the well-established laser Doppler velocimetry to allow the simultaneous measurement of size and velocity of individual droplets crossing a defined region in space. The results show the high resolution with which the system can measure droplets of different size classes. This is expected given that for this technique the resolution is constant throughout the size spectrum. The accuracy of the system is satisfactory for engineering purposes (~10%), but it still remains to be seen why the measured sizes were consistently smaller than the predicted sizes by ~8%. Part of this error can be attributed to the finite size of the beams, as discussed in the paper for a size range of 10; this is ~3%.

Signal-to-noise considerations indicate that the dynamic size range capability of the instrument can be in excess of 100:1. However, practical limitations in the electronics and the need to make measurements in high number density flows indicate that a more realistic dynamic size range is 30:1. The capability to measure velocity is based on the well-established LDV concept. The big advantage offered by this system is the ability to measure simultaneously the size and velocity of individual droplets with high resolution over a large dynamic range.

Also, it is expected that particles of slight irregular shape can be measured with this system by collecting and analyzing the diffracted component of the scattered light.

References

1. A. J. Yule, N. A. Chigier, S. Atakan, and A. Ungut, "Particle Size and Velocity Measurement by Laser Anemometry," J. Energy **1**, 220 (1977).
2. D. Holve and S. A. Self, "Optical Particle Sizing for *In Situ* Measurements," Appl. Opt. **18**, 1632 (1979).
3. Y. Mizutani, H. Kodama, and K. Miyasaka, "Doppler-Mie Combination Technique for Determination of Size-Velocity Correlation of Spray Droplets," Combust. Flame **44**, 85 (1982).
4. A. Men, Y. Krimerman, and D. Adler, "A New Method of Simultaneous Particle Sizing and Two-Component Velocity Measurement," J. Phys. E. **14**, 747 (1981).
5. P. R. Ereaut, A. Ungut, A. J. Yule, and N. Chigier, "Measurement of Drop Size and Velocity in Vaporizing Sprays," in *Proceedings, Second International Conference of Liquid Atomization and Spray Systems, Madison, Wisc. (20–24 June 1982)*, p. 261.
6. W. J. Glantschnig, M. W. Golay, S.-H. Chen, and F. R. Best, "Light Scattering Device for Sizing and Velocimetry of Large Droplets Utilizing a Ring-Shaped Laser Beam," Appl. Opt. **21**, 2456 (1982).
7. M. L. Yeoman, B. J. Azzopardi, H. J. White, C. J. Bates, and P. J. Roberts, "Optical Development and Application of a Two Color LDA System for the Simultaneous Measurement of Particle Size and Particle Velocity," in *Engineering Applications of Laser Velocimetry*, Winter Annual Meeting ASME, Phoenix, Ariz., 14–19 Nov. 1982.
8. C. F. Hess, "A Technique Combining the Visibility of a Doppler Signal with a Peak Intensity of the Pedestal to Measure the Size and Velocity of Droplets in a Spray," in AIAA Twenty-Second Aerospace Sciences Meeting, 84-0203, Reno, Nev., 9–12 Jan. 1984.
9. H. C. van de Hulst, *Light Scattering by Small Particles* (Wiley, New York, 1957), Chap.12.
10. D. W. Roberts, C. W. Brasier, and B. W. Bomar, "Use of a Particle Sizing Interferometer to Study Water Droplet Size Distribution," Opt. Eng. **18**, No. 3, 236 (1979).
11. B. Y. H. Liu, R. N. Berglund, and T. K. Argawal, "Experimental Studies of Optical Particle Counters," Atmos. Environ. **18**, 717 (1974).

This work was supported by the Combustion Fundamentals Section of NASA Lewis under contract NAS3-23538 and the Air Force Office of Scientific Research (AFOSR) under contract F49620-83-C-0060.

The author is also grateful for the technical contributions of Anthony Smart, Tom Hunt, Dariush Modarress, and Victor Espinosa.

APPENDIX B

A reprint from

Optical Engineering

23(5), 604-609 (September/October 1984).

ISSN 0091-3286

SPRAY CHARACTERIZATION WITH A NONINTRUSIVE TECHNIQUE USING ABSOLUTE SCATTERED LIGHT

Cecil F. Hess
Victor E. Espinosa

Spectron Development Laboratories
3303 Harbor Boulevard
Suite G-3
Costa Mesa, California 92626

Spray characterization with a nonintrusive technique using absolute scattered light

Cecil F. Hess
Victor E. Espinosa
Spectron Development Laboratories
3303 Harbor Boulevard
Suite G-3
Costa Mesa, California 92626

Abstract. A technique to measure the size and velocity of particles is discussed, and results are presented. In this technique two small laser beams of one color identify the center of a laser beam of a different color. This defines a region of almost uniform intensity where the light scattered by the individual particles can be related to their sizes. A variation of this technique that uses two polarizations of the same color of laser beam is also presented. Results are presented for monodisperse, bimodal, trimodal, and polydisperse sprays produced by the Berglund-Liu droplet generator and a pressure nozzle. Size distributions obtained at three different ranges for the same spray show excellent self-consistency in the overlapping regions. Measurements of a spray of known characteristics exhibit errors in the order of 10%.

Keywords: particle sizing and spray analysis; spray characterization; scattered light; polarization.

Optical Engineering 23(5), 604-609 (September/October 1984).

CONTENTS

1. Introduction
2. Theoretical approach
3. Error analysis
4. Self-calibrating algorithm
5. Probe volume
6. Description of apparatus
   6.1. Advanced Droplet Sizing System
   6.2. PIMAX system
7. Results
8. Effect of beam blockage on size distribution
9. Acknowledgments
10. References

1. INTRODUCTION

This paper discusses some of the theoretical aspects and results obtained with a novel technique to measure nonintrusively and in real time the size and velocity of droplets in a spray. The method, referred to as IMAX (intensity maximum), bases the size measurement on the absolute intensity of the light scattered by individual droplets crossing an illuminated probe volume. The velocity is obtained from the Doppler signal using the standard laser Doppler velocimeter (LDV) approach.

The probe volume of the IMAX technique is shown in Fig. 1. Two small laser beams of one wavelength are crossed in the middle of a larger laser beam of another wavelength. Thus, an interferometric pattern of fringes is formed in the crossover, defining a region of almost uniform intensity within the large beam. The theoretical details of this technique are shown in Ref. 1. The work presented here will show the results obtained recently with IMAX and will describe in detail the effect of using Gaussian beams in the signal detectability. We will also describe an apparatus designed and built based on the IMAX technique, and finally we will discuss some preliminary work showing the feasibility of using laser beams with two polarizations instead of two wavelengths.

Several nonintrusive single particle counters have been proposed, which can be divided into two groups. In the first group[2-4] Gaussian laser beams are used, and various mathematical inversion techniques have been proposed to extract the true size distribution from the signal amplitude distribution. The second group[5-8] uses a probe volume of known illumination to avoid the ambiguity of particle position. The technique described here falls in this group. Some of the distinct advantages of the IMAX technique are that (1) it requires no special mask that may alter the signal; (2) it uses stable TEM_{oo} laser beams; (3) combined with the visibility of the fringe pattern, it provides a self-calibrating technique; and (4) it is characterized by a large dynamic size range (dynamic ranges in excess of 30 are expected after developing the proper electronics).

Invited Paper PS-107 received March 10, 1984; revised manuscript received May 7, 1984; accepted for publication May 8, 1984; received by Managing Editor May 29, 1984.

2. THEORETICAL APPROACH

The mathematical model is for spherical particles much larger than the wavelength of the incident laser beams.

If we refer to the small beams as 1 and the large beam as 2, the intensity of the light scattered by a spherical particle is given by

$$I_{s_1} = 2I_{o_1}K_{o_1}\,d^2 \exp\left[\left(-\frac{2}{b_{o_1}^2}\right)(x^2+y^2)\right] \times \left(1+\cos 2\frac{\pi\gamma x}{\lambda}V\right), \quad (1)$$

and

$$I_{s_2} = I_{o_2}K_{o_2}\,d^2 \exp\left[\left(-\frac{2}{b_{o_2}^2}\right)(x^2+y^2)\right], \quad (2)$$

where I_o is the central intensity of the incident beam, K_o is the scattering coefficient, d is the particle diameter, b_o is the waist radius, λ is the wavelength, V is the particle visibility, and x, y are the coordinates. It has been assumed that the intensity variation with z is negligible. The scattering coefficient is the sum of refraction, reflection, and diffraction terms.[9]

These contributions are, in general, functions of the collection angle and the particle size.

The ac modulation of I_{s_1} is used to establish the detectability of the signal and to measure the velocity. The peak of I_{s_2} establishes the size.

Equations (1) and (2) apply to the two-color or the two-polarization concepts. The difference will be established in the computation of the scattering coefficients.

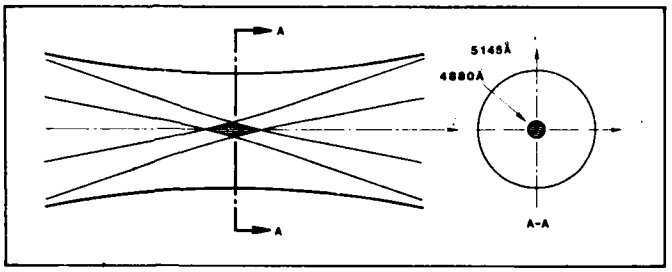

Fig. 1. Probe volume of the two-color IMAX technique.

TABLE I. Size Errors for Different Beam Ratios and Dynamic Size Ranges

Beam ratio	d_{max}/d_{min}	Max error
7	10	3%
7	20	4%
7	30	5%
5	10	5%
5	20	8%
5	30	10%

3. ERROR ANALYSIS

There are several sources of error in the IMAX method that must be considered to properly design an instrument. The method requires a single particle in the probe volume, adequate signal-to-noise ratio for a large dynamic range, known particle illumination, and, in general, spherical particles.

The first two sources of error are discussed in LDV papers. The requirement of knowing the illumination on the particle is characteristic of methods that base the size on the absolute scattered light. There are two known sources of error in establishing the particle illumination. First is the attenuation resulting from beam blockage produced by other particles in the trajectory of the transmitted and scattered light. For fuel nozzles this is typically between 10% and 30%, and if this attenuation is known the gain of the photodetectors can be adjusted to compensate for it.

Broadening that results from random beam blockage, however, cannot be corrected. Interestingly enough, this broadening is not only the result of beam blockage but also of reradiation into the probe volume. Tests conducted with stationary targets and monodisperse droplets show that beam blockage produces an average attenuation and some broadening of lower and higher amplitude signals. In highly fluctuating sprays, however, it is conceivable that the attenuation will change very rapidly, thus introducing errors.

In the next section we discuss a method to establish and correct for all sources of attenuation.

The second error source is that, since the small beam has a finite diameter, the particles can travel a small distance away from the center of the big beam and still cross sufficient fringes to be detectable. The farther from the center a particle can be detected, the larger the error it can produce. This error increases directly with dynamic size range and inversely with the ratio of the large to small beams. Table I shows the errors that can be incurred due to the Gaussian nature of the small and large beams.

4. SELF-CALIBRATING ALGORITHM

Single particle counters based on absolute scattered light require calibration at one datum point. When measuring dense sprays, beam attenuation will make this calibration difficult. An algorithm is discussed here that will eliminate this problem.

The algorithm is based on measuring the visibility of any size class droplet. Combining the visibility and intensity[10] of the signal, a very accurate measurement of a given size can be made. Notice that the visibility intensity technique can be used very accurately to measure a very narrow size range. Knowing the size of the chosen corresponding visibility, one can then establish the amplitude of the pedestal of this signal by adjusting the gain to the photodetector. The logic is as follows: for a given visibility (chosen in the most accurate region of the visibility function) there is an associated size and, therefore, an intensity scattered from the large beam. Since the intensity of this large beam is almost uniform, the scattered light associated with the chosen visibility will be almost constant in the absence of errors in the visibility. There are, however, errors associated with measuring visibility in a dense spray, and these points are rejected by V/I.[10] The process is an iterative one in which V/I is implemented by choosing several narrow intensity bands to establish points out of control. The gain to the photodetector is adjusted until the majority of the points fall in the preestablished intensity band corresponding to the measured size.

This algorithm, however, imposes restrictions to the IMAX technique. To relate size to visibility, the fringe spacing (δ) and the collection factor (CF) (established by the index of refraction, solid angle of collection, and wavelength) must follow the relationship

$$\frac{d_{max}}{\delta CF} = 0.845 \ , \tag{3}$$

where d_{max} is the largest particle of interest.

There are also restrictions associated with the number of fringes to the e^{-2} intensity of the small beams (typically 8 to 20).

The self-calibrating algorithm has been successfully used in the Advanced Droplet Sizing System described in a later section.

5. PROBE VOLUME

Particles that scatter light with large modulation are detectable over a larger region than those that scatter light with little modulation. As a result, the probe volume or region of detectability is a function of droplet size. A very simple algorithm is discussed in Ref. 1 for the two-color system and off-axis collection. Results showing raw and corrected data for a spray are presented in the next section.

To correct raw data obtained with Gaussian beams and off-axis collection with limiting apertures, it is necessary to know only the dimension (y) normal to the particle trajectory and the beam bisector, given by

$$y \leq \sqrt{-\frac{b_{o_1}^2}{2} \ell n \left[\frac{I_{min}}{2I_{max}} \left(\frac{d_o}{d} \right)^2 \frac{(1 + V_o)}{V} \right] - b_{o_1}^2} \ , \tag{4}$$

where I_{min} is the intensity threshold and I_{max} is the saturation level established by the electronics, d_o produces the largest signal within the detectable range, and V_o is its corresponding visibility.

Because of the multivalued characteristic of the visibility curve, V_o should be larger than the first zero of the visibility function. Equation (3) defines the abscissa of this function as $d' = d/(\delta CF)$. This value should be kept smaller than one; however, physical constraints render this not always possible. The collection factor (CF) can be easily changed almost linearly by changing the aperture f number of the collecting lens. In the experiments reported here this was done by placing a mask on the path of light scattered by the small beams. As an example, the spray data shown in Figs. 8(a) and 9(a) correspond to $I_{min} = 0.6 \times 10^{-3}$ V and $I_{max} = 0.7$ V (these intensities are read directly in volts). Since very little data were measured above 160 μm, the mask was chosen to obtain $d' = 1$ at about 160 μm. Therefore,

$$d_o' = \frac{200}{\delta CF} = \frac{200}{160} = 1.24 \ . \tag{5}$$

Table II shows values obtained for the nondimensional diameter (d'),

TABLE II. Typical Values Obtained for the Nondimensional Diameter (d'), Its Visibility (V), and the Normal Probe Volume Dimension (y) for Three Sizes Ranges

	Size range: 20 to 200 μm									
d	20	40	60	80	100	120	140	160	180	200
d'	0.12	0.25	0.37	0.5	0.62	0.75	0.87	1	1.12	1.24
V	0.97	0.88	0.76	0.6	0.43	0.27	0.12	0.02	0.08	0.12
y	0.35	0.9	1.06	1.14	1.17	1.15	1.03	0.55	1.05	1.19

	Size range: 10 to 100 μm					Size range: 5 to 50 μm				
d	20	40	60	80	100	10	20	30	40	50
d'	0.2	0.4	0.6	0.8	1	0.19	0.38	0.57	0.76	0.95
V	0.92	0.73	0.46	0.2	0.02	0.93	0.76	0.51	0.24	0.04
y	0.93	1.2	1.27	1.22	0.75	0.93	1.2	1.29	1.25	0.95

its visibility (V), and the normal probe volume dimension [y, as given by Eq. (4)].

In establishing the various size ranges the procedure used was to adjust the gain of the photomultiplier tubes (PMTs) until the maximum size of the range of interest (200, 100, and 50 μm, respectively) exhibited a peak amplitude $I_{max} = 0.7$ V. The receiving aperture was selected to produce adequate ac modulation to ensure the detectability of all the drops within the size range. Typically, the visibility of the largest droplet of any size range was about 0.02. Notice that with these criteria we must expect that the probe volume of the 20 μm droplet (as an example) is larger in the 5 to 50 μm range than in the 20 to 200 μm range.

6. DESCRIPTION OF APPARATUS

Three systems have been used throughout the work presented here. The first is a two-color IMAX breadboard,[1] the second is an apparatus designed and built for NASA Lewis (Fundamental Combustion Section) and referred to as the Advanced Droplet Sizing System (ADSS), and the third consists of a breadboard employing the two-polarization signal color PIMAX (polarization intensity maximum) technique. In this section we will describe the last two systems.

6.1. ADSS

Figure 2 shows the transmitter and receiver. The transmitter houses an argon-ion laser, which provides the light source, and all the required optics to separate the two colors used (5145 and 4800 Å) to form the probe volume of interest. The receiver is essentially a telescope with two photomultipliers to collect the light scattered by particles crossing the sample volume. This beam is split in two via a beam splitter and a mirror system; each beam is focused on the pinhole of the corresponding PMT housing. The colors are separated by means of narrow-band filters internal to the PMT housings. The outputs of the two PMTs are then electronically processed, and information about the size and velocity of individual spheres crossing the probe volume is thus obtained. An electronic processor was developed for this purpose, and a dedicated microprocessor was interfaced to store, display, and analyze the acquired data. Sample rates of several kHz are possible with this system. Figure 3 shows the electronic equipment used for data processing. It should be noted that the system uses a VP-1001 processor and a newly developed V-I IMAX interface.

6.2. PIMAX system

Figure 4 shows the optical setup used for the PIMAX system. A helium-neon laser provides the light source of wavelength 6328 Å. A Wollaston prism splits the laser beam into two beams with S and P polarization. The intensity ratio of these two beams can be adjusted with a polarization rotator placed just before the Wollaston prism.

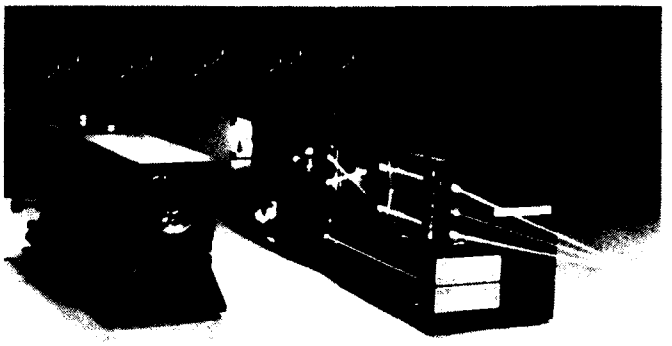

Fig. 2. Transmitter and receiver units of the Advanced Droplet Sizing System (ADSS) used for IMAX measurements.

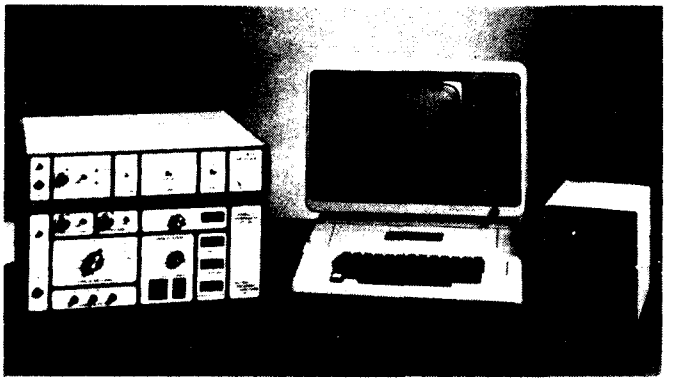

Fig. 3. Photograph of the ADSS electronics.

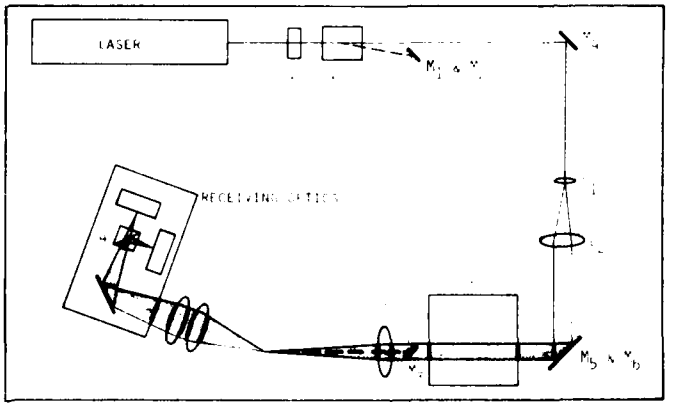

Fig. 4. Schematic of the PIMAX breadboard: (1) polarization rotator; (2) Wollaston prism; (3) beam splitter unit; (4) cube polarizing beam splitter.

One of these beams is then expanded with the use of lenses L_1 and L_2, which act as a beam expander, thus achieving the beam ratio parameter m. This expanded beam is then split into two beams by using a compensated beam splitter. The transmitting lens L_3 focuses and crosses these two beams (which will be referred to as small beams because of their size at the probe volume relative to the third beam), thus forming an interference pattern of fringes in the middle of the big beam.

The scattered light collected by the receiver is separated into the P and S components by a cube polarizing beam splitter and is focused on pinholes in front of two identical PMTs. Interference filters are used to eliminate background light from other sources.

7. RESULTS

Spray measurements are reported for two kinds of atomizers. The first is a Berglund-Liu droplet generator, and the second is a Spray Systems pressure nozzle TG0.3.

The Berglund-Liu droplet generator was used to produce strings and sprays of known size droplets. This generator produces a string of droplets of equal size and spacing. These droplets can be dispersed with external air to produce a spray of monodispersed droplets, or under some dispersion conditions the primary droplets will collide and form doublets and triplets.[11] The procedure used in these experiments was to produce a string of large monodispersed droplets to calibrate the instrument. Smaller droplets were then produced by increasing the frequency of vibration of the orifice, and with the dispersion air a spray of these droplets was formed. The spray angle was about 10°, and the number density was typically 500/cm^3. The optical configuration consisted of a transmitting lens of 711 mm, beam ratio of m = 7, small beam diameter of 100 μm, receiving angle of 20°, and receiving lenses of 300/495 mm. The calibration point was provided by a string of 100 μm droplets produced with a flow rate of 0.21 cm^3/min and a frequency of 5 kHz. Figure 5 shows the measured size and velocity. A spray of primary droplets of 49 μm (produced with a flow rate of 0.21 cm^3/min and frequency of 56.9 kHz) was then produced with the dispersion air. Figure 6(a) shows the measurements of a spray of primary droplets. Figure 6(b) shows the measurements of a spray formed of primary droplets and doublets. The theoretically predicted sizes are 49 and 62 μm. The sizes actually measured were 46 and 57 μm, respectively. Figure 6(c) extends the measurements of Fig. 6(b) to the presence of triplets. The theoretically predicted sizes in this case are 49, 62, and 70 μm. Note that the measured diameters of the doublets and triplets are related to the primary droplets by $2^{1/3}$ and $3^{1/3}$, respectively.

In the absence of a true standard spray it was difficult to establish how much of the measured error (which was about 8%) could be attributed to the measuring technique and how much to the flow rate through the piezoelectric driven orifice. A pressure gauge placed between the orifice and the syringe pump showed that there existed long-term variations in the pressure.

8. EFFECT OF BEAM BLOCKAGE ON SIZE DISTRIBUTION

The effect on the size distribution of spray blocking the laser beams before they cross was measured with IMAX. A size range of 10 to 100 μm was used in this case, and the monodispersed droplet size was 73 μm.

Figure 7(a) shows the measurement of the monodispersed string of droplets. Figure 7(b) shows similar results, but a spray is blocking

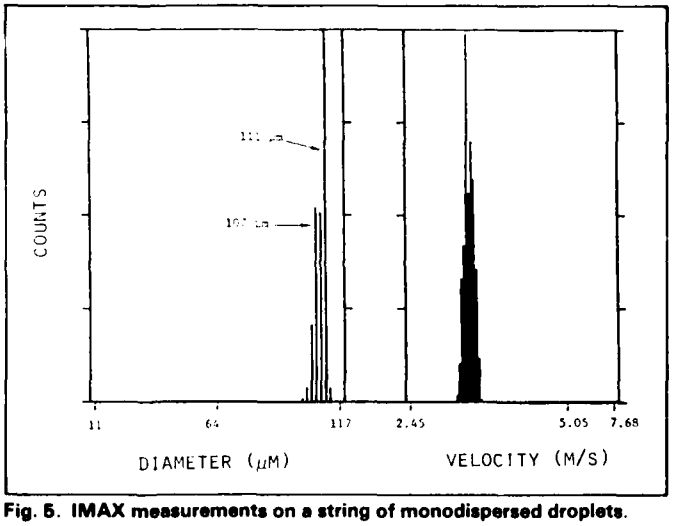

Fig. 5. IMAX measurements on a string of monodispersed droplets.

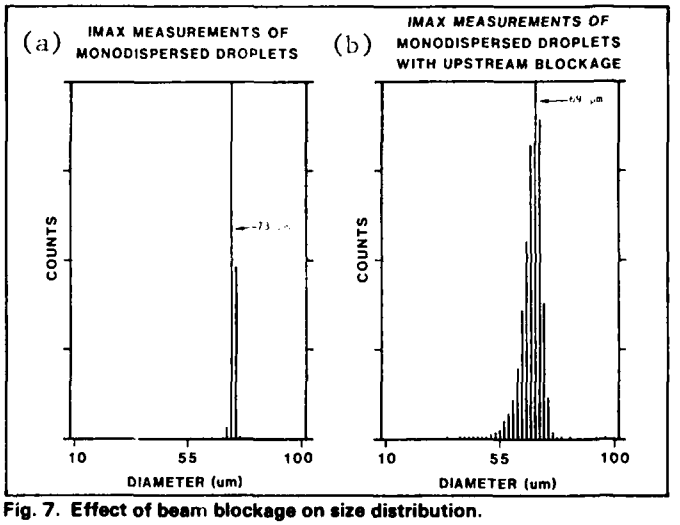

Fig. 7. Effect of beam blockage on size distribution.

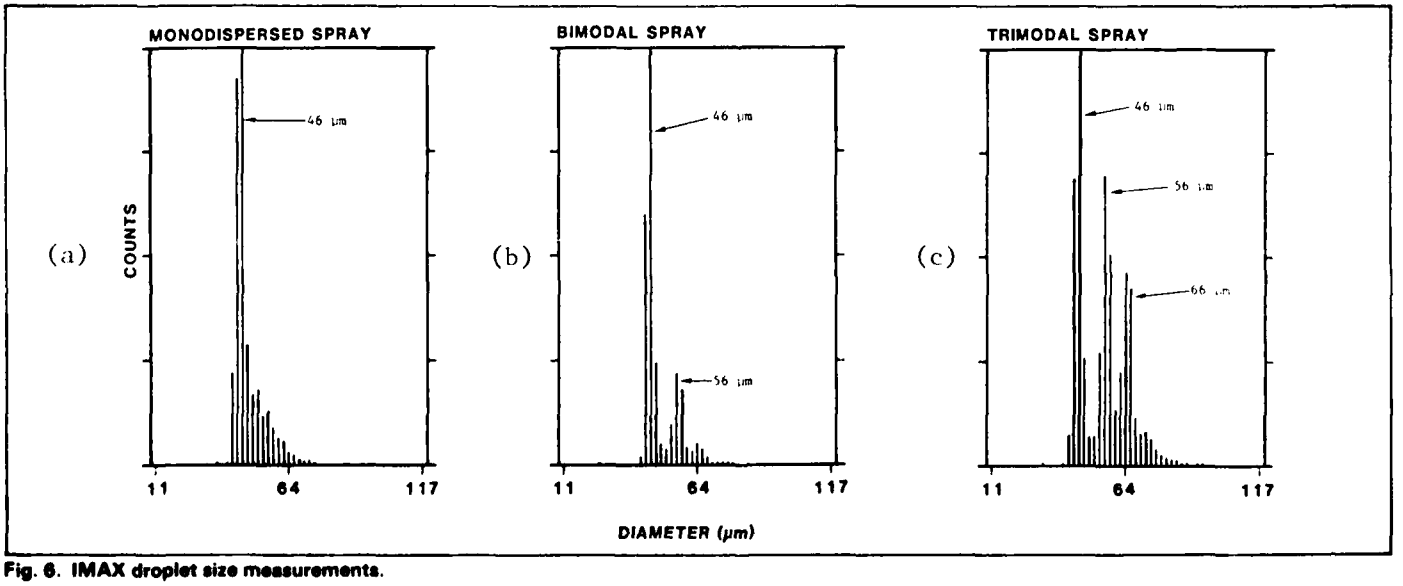

Fig. 6. IMAX droplet size measurements.

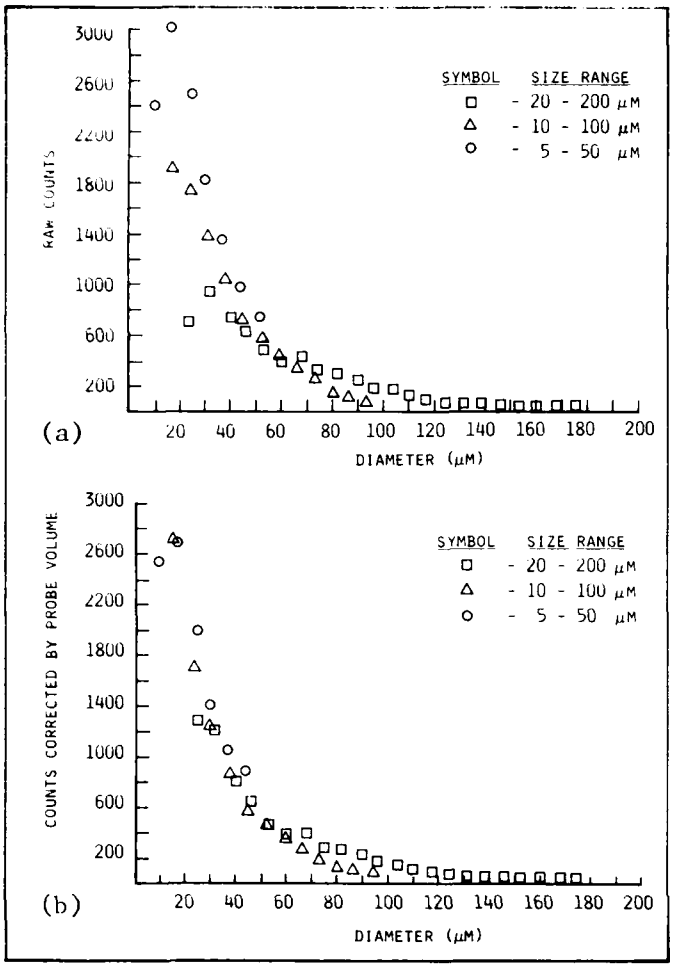

Fig. 8. IMAX measurements of a spray at a radial position of 0 mm: (a) uncorrected size distribution and (b) probe volume corrected size distribution.

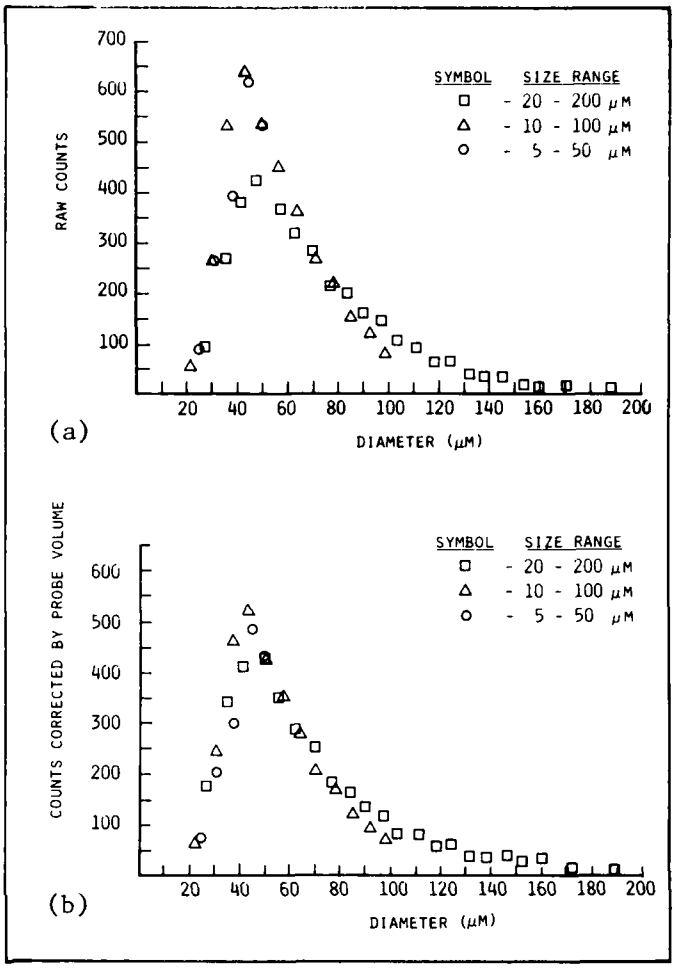

Fig. 9. IMAX measurements of a spray at a radial position of 10 mm: (a) uncorrected size distribution and (b) probe volume corrected size distribution.

the laser beam. Two effects can be noted: the peak of the distribution dropped to 69 μm (5%), and the spread of the distribution is +5 μm, −7 μm (+7%, −10%) to the $1/e^2$. It should be noted that once the high voltage is corrected to account for the beam blockage, the broadening should have very little effect on the distribution of a polydisperse spray.

The following results correspond to a spray produced by a pressure nozzle (Spray Systems TG0.3 at 50 psi and 50 mm from the tip). These results are adequate to show trends and gross changes in the distributions. However, considerable transient variations were observed in both the size and velocity distributions. These variations were the result of changes in the spray pattern produced by the above-mentioned nozzle. Simple visual observations of the spray pattern indicated changes from conical to flattened sprays. Nevertheless, recognizing that a standard invariable spray is not available, we proceeded to make measurements that would allow us to test the probe volume algorithm and to compare the two-color IMAX with the two-polarization IMAX (referred to as PIMAX).

The first sets of measurements are shown in Figs. 8(a), 8(b), 9(a), and 9(b). They were made at a radial position of 0 and 10 mm. Figures 8(a) and 9(a) show the raw data, while Figs. 8(b) and 9(b) show the probe volume corrected data. Comparing the raw and the probe volume corrected data, it is quite apparent how signal detectability influences the number of counts in the histograms. For instance, the ability to detect a 25 μm droplet with a size range of 20 to 200 μm is much more limited than with a size range of 5 to 50 μm. This change in sensitivity is what the probe volume is all about, and it is characteristic of any optical technique (for instance, in photography the data rate must be corrected by the depth of field).

The trend shown in Figs. 8(b) and 9(b) is the expected one. That is, there are more small droplets in the middle of the spray than on the edge.

In order to test the resolution of the system, data were obtained using three different size ranges: 5 to 50 μm, 10 to 100 μm and 20 to 200 μm. This is one of the most difficult self-consistency tests imposed on any technique, and most available techniques will show a shift in the predicted data. IMAX shows excellent matching of the data in the overlapping region, as illustrated in Figs. 8(b) and 9(b).

Measurements were also made to compare the data obtained with the two-color ADSS and the two-polarization PIMAX system. These measurements were performed at approximately the same locations as before but with a time difference of one month. Notice that some variations are expected due to changes in the spray pattern. The size distributions obtained with the ADSS system and the PIMAX breadboard are shown in Fig. 10(a) (radius = 0), and Fig. 11(a) (radius = 10 mm). The corresponding velocity distributions are shown in Figs. 10(b) and 11(b). The results of both systems agree very strongly with the expected trend. That is, more smaller particles were measured at the center of the spray than at the edge. This is illustrated in Figs. 10(a) and 11(a). Furthermore, since small particles move slower than large ones, the average velocity of particles at the center of the spray is expected to be smaller than the corresponding velocity at the edge, where large particles are predominant. This can be verified if reference is made to Figs. 10(b) and 11(b) (notice the

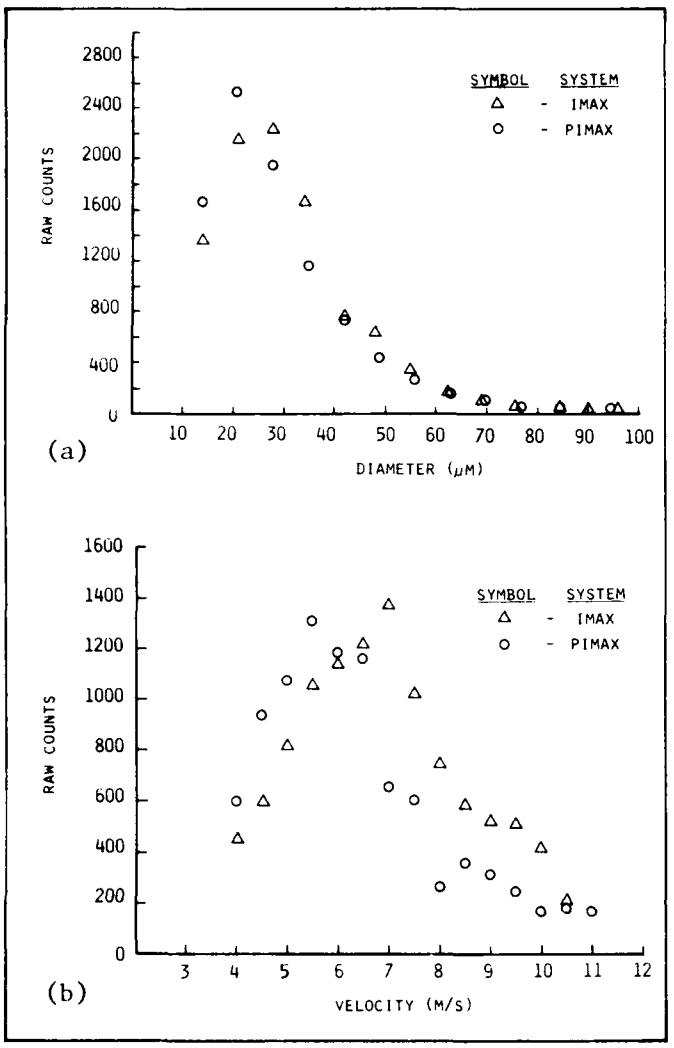

Fig. 10. (a) Particle size distribution and (b) particle velocity distribution using IMAX and PIMAX systems. Radial position of the spray is 0 mm.

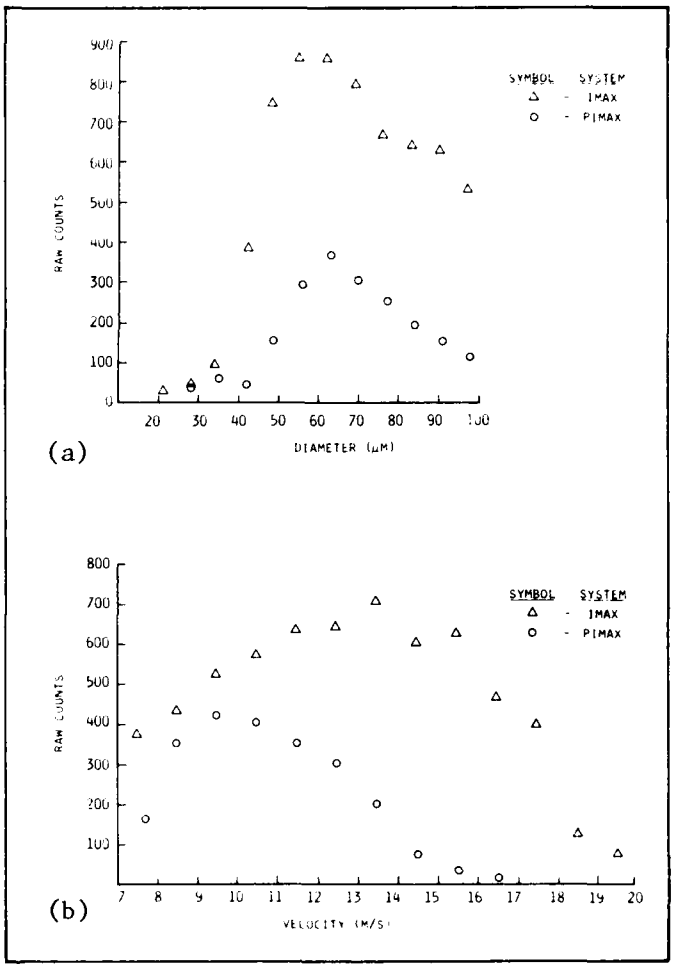

Fig. 11. (a) Particle size distribution and (b) particle velocity distribution using IMAX and PIMAX systems. Radial position of the spray is 10 mm.

change in scale). Several runs taken with both systems indicate that the IMAX and PIMAX systems are in agreement. However, for descriptive purposes only, representative runs for each mode are presented.

Very good agreement in the size distributions obtained with both systems is shown in Fig. 10(a). Slightly larger particles were measured with IMAX, which is also evidenced by the velocity distributions shown in Fig. 10(b). That is, faster moving particles were measured with IMAX. This effect was more pronounced at the 10 mm position [Figs. 11(a) and 11(b)] and reflects a considerable change of the spray pattern. Notice that at the 10 mm position the size distributions [Fig. 11(a)] are similar but the number of counts is considerably different. This may be the result of a change in local number density resulting from the change in spray pattern. As before, this change is also observed in the velocity distributions [Fig. 11(b)], which show faster moving events measured with IMAX. It should be pointed out that previous and extensive experimentation with this particular spray nozzle using IMAX did indeed show some fluctuation in the data rate. Also, since there was a time gap of about one month between measurements taken with IMAX and PIMAX, much of the discrepancy in data rate may be attributed to an internal change in the spray nozzle. It has been planned at the time of writing this paper to conduct tests with both systems within a shorter time gap and possibly with a more stable nozzle to minimize causes of data rate discrepancy.

9. ACKNOWLEDGMENTS

This work was supported by the Air Force Office of Scientific Research (AFOSR) under Contract No. F49620-83-C-0060 and the Combustion Fundamentals Section of NASA Lewis under Contract No. NAS3-23538.

The authors are also grateful for the technical contributions of Anthony Smart, Tom Hunt, and Roger Rickey, who engineered and built the ADSS.

10. REFERENCES

1. C. F. Hess, "A Nonintrusive Optical Single Particle Counter for Measuring the Size and Velocity of Droplets in a Spray." Submitted to Appl. Opt.
2. A. J. Yule, N. A. Chigier, S. Atakan, and A. Ungut, J. Energy 1, 220 (1977).
3. D. Holve and S. A. Self, Appl. Opt. 18, 1632 (1979).
4. Y. Mizutani, H. Kodama, and K. Miyasaka, *Combustion and Flame* 44, 85 (1982).
5. A. Men', Y. Krimerman, and D. Adler, J. Phys. E. 14, 747 (1981).
6. P. R. Ereaut, A. Ungut, A. J. Yule, and N. Chigier, Proc. 2nd Int. Conf. of Liquid Atomization and Spray Systems, p. 261 (1982).
7. W. Glantschnig, M. W. Golay, S-H. Chen, and F. R. Best, Appl. Opt. 21, 2456 (1982).
8. M. L. Yeoman, B. J. Azzopardi, H. J. White, C. J. Bates, and P. J. Roberts, *Eng. Appl. of Laser Velocimetry*, Winter Annual Meeting ASME (1982).
9. H. C. van de Hultz, *Light Scattering by Small Particles*, Chap. 12, John Wiley and Sons, New York (1957).
10. C. F. Hess, AIAA 22nd Aerospace Sciences Meeting, AIAA-84-0203 (1984).
11. B. Y. H. Liu, R. N. Berglund, and T. K. Argawal, Atmospheric Environment 8, 717 (1974).

END

FILMED

10-85

DTIC